Available online at www.sciencedirect.com
SCIENCE DIRECT®
Journal of Sound and Vibration 272 (2004) 703–730
JOURNAL OF SOUND AND VIBRATION
www.elsevier.com/locate/jsvi

Three-dimensional exact solution for the vibration of functionally graded rectangular plates

Senthil S. Vel[a,*], R.C. Batra[b]

[a] *Department of Mechanical Engineering, University of Maine, 5711, Boardman Hall room 214, Orono, ME 04469-5711, USA*

[b] *Department of Engineering Science and Mechanics, M/C 0219, Virginia Polytechnic Institute and State University Blacksburg, VA 24061, USA*

Received 1 February 2002; accepted 3 April 2003

Abstract

A three-dimensional exact solution is presented for free and forced vibrations of simply supported functionally graded rectangular plates. Suitable displacement functions that identically satisfy boundary conditions are used to reduce equations governing steady state vibrations of a plate to a set of coupled ordinary differential equations, which are then solved by employing the power series method. The exact solution is valid for thick and thin plates, and for arbitrary variation of material properties in the thickness direction. Results are presented for two-constituent metal–ceramic functionally graded rectangular plates that have a power-law through-the-thickness variation of the volume fractions of the constituents. The effective material properties at a point are estimated by either the Mori–Tanaka or the self-consistent schemes. Exact natural frequencies, displacements and stresses are used to assess the accuracy of the classical plate theory, the first order shear deformation theory and a third order shear deformation theory for functionally graded plates. Parametric studies are performed for varying ceramic volume fractions, volume fraction profiles and length-to-thickness ratios. Results are also computed for a functionally graded plate that has a varying microstructure in the thickness direction using a combination of the Mori–Tanaka and the self-consistent methods. Forced vibrations of a plate with a sinusoidal spatial variation of the pressure applied on its top surface are scrutinized.

1. Introduction

The superior properties of advanced composite materials, such as high specific strength and high specific stiffness, have led to their widespread use in aircrafts, spacecrafts and space

*Corresponding author. Tel.: +1-207-581-2777; fax: +1-207-581-2379.
E-mail address: senthil.vel@maine.edu (S.S. Vel).

0022-460X/03/$ - see front matter
doi:10.1016/S0022-460X(03)00412-7

structures. In conventional laminated composite structures, homogeneous elastic laminae are bonded together to obtain enhanced mechanical and thermal properties. However, the abrupt change in material properties across the interface between different materials can result in large interlaminar stresses leading to delamination. Furthermore, large plastic deformations at the interface may trigger the initiation and propagation of cracks in the material. One way to overcome these adverse effects is to use "functionally graded materials" in which material properties vary continuously. This is achieved either by gradually changing the volume fraction of the constituent materials, usually in the thickness direction only, or by changing the chemical structure of a thin polymer sheet to obtain a smooth variation of in-plane material properties and an optimum response to external thermomechanical loads. The former class of functionally graded structures can be manufactured by high speed centrifugal casting [1,2] in which layers are formed in the radial direction due to different mass densities of the constituents, or by depositing layers of ceramic materials on a metallic substrate [3,4]. Lambros et al. [5] have developed an ultraviolet irradiation process to obtain variations in Young's modulus in the plane of a sheet. A directed oxidation technique has been employed by Breval et al. [6] and Manor et al. [7] to obtain a ceramic layer on the outside surface.

Several studies have been performed to analyze the behavior of functionally graded plates and shells. Reddy [8] has analyzed the static behavior of functionally graded rectangular plates based on a third-order shear deformation plate theory. Cheng and Batra [9] have related deflections of a simply supported functionally graded polygonal plate given by a first order shear deformation theory and a third order shear deformation theory to that of an equivalent homogeneous Kirchhoff plate. Cheng and Batra [10] have also presented results for the buckling and steady state vibrations of a simply supported functionally graded polygonal plate based on Reddy's plate theory. Loy et al. [11] have studied the vibration of functionally graded cylindrical shells using Love's shell theory. Batra [12] analyzed finite plane strain deformations of a circular cylinder made of a Mooney–Rivlin material with the two material parameters depending upon the radial co-ordinate.

Although there are several three-dimensional (3-D) solutions available for inhomogeneous plates, most of these studies are for laminated plates consisting of homogeneous laminae. Analytical 3-D solutions for plates are useful since they provide benchmark results to assess the accuracy of various 2-D plate theories and finite element formulations. Exact analytical solutions for the bending, vibration and buckling of homogeneous and laminated thick rectangular plates were developed by Srinivas et al. [13–15]. Rogers et al. [16] have employed the method of asymptotic expansion to analyze 3-D static deformations of inhomogeneous plates. However, the boundary conditions on the edges of the plate in their theory are applied in an average sense like those in 2-D plate theories and the plate is assumed to be only moderately thick. Tarn and Wang [17] have also presented an asymptotic solution that may be carried out to any order, but the manipulations become more and more involved as one considers higher order terms, and numerical examples are given only for laminated plates consisting of homogeneous layers. Cheng and Batra [18], and Reddy and Cheng [19,20] have also used the method of asymptotic expansion to study the 3-D thermoelastic deformations of a functionally graded elliptic and rectangular plates respectively. If boundary layer effects near the clamped and free edges can be neglected, then the asymptotic expansion methods can also be applied to study plate problems for different edge conditions. For thick plates, boundary layers are also prevalent adjacent to the top and the

bottom surfaces of the plate; e.g. see Vel and Batra [21]. These may not be well captured by the method of asymptotic expansion. Lee et al. [22,23] have expanded the mechanical displacements, electric potential and the material moduli as power series in the thickness co-ordinate and derived plate equations of different orders for functionally graded piezoelectric disks, infinite plates and strips. Recently, Vel and Batra [24,25] presented an exact 3-D solution for the thermoelastic deformation of functionally graded simply supported plates. Qian et al. [26] have employed a higher order shear and normal deformable plate theory of Batra and Vidoli [27] and a meshless local Petrov–Galerkin method proposed by Atluri and Zhu [28] to analyze static and dynamic deformations of a functionally graded plate. The computed results agree very well with the analytical solutions presented herein and in Vel and Batra [24]. Reiter et al. [29] and Reiter and Dvorak [30,31] have performed detailed finite element studies of discrete models containing simulated particulate and skeletal microstructures and compared results with those computed from homogenized models in which effective properties were derived by the Mori–Tanaka [32,33] and the self-consistent [34] methods. Jin and Batra [35–37] used the 3-phase model [38,39] to deduce the effective moduli of a 2-constituent composite and employed a quasistatic linear thermoelasticity theory to analyze fracture characteristics of a functionally graded plate.

The objective of this investigation is to present an exact solution for the vibration of simply supported rectangular thick plates. We assume that the plate is made of an isotropic material with material properties varying in the thickness direction only. By using suitable displacement functions, the governing partial differential equations are reduced to a set of coupled ordinary differential equations in the thickness direction, which are then solved by the power series method. Numerical results are presented for a two-phase graded material with a power-law through-the-thickness variation of the volume fractions of the constituents. The effective material properties at a point are estimated from the local volume fractions and the material properties of the phases either by the Mori–Tanaka [32,33] or the self-consistent [34] scheme. Results are presented for an aluminum/zirconia graded rectangular plate. Natural frequencies, displacements and stresses are given for various length-to-thickness ratios, the exponent in the power-law that describes through-the-thickness variation of the constituents and different homogenization schemes. We compare exact results with those obtained from the classical plate theory (CPT) [40], the first order shear deformation theory (FSDT) [41,42] and a third order shear deformation theory (TSDT) [43]. Results are also presented for a functionally graded plate that has a particulate microstructure near the lower metal-rich and the upper ceramic-rich surfaces and a skeletal microstructure in between. The effective material properties in the region with skeletal microstructure are obtained using the self-consistent scheme and properties for the region with particulate microstructures are estimated by the Mori–Tanaka scheme. Forced vibrations of a plate with a pressure load applied on its top surface have also been analyzed.

2. Problem formulation

We use rectangular Cartesian co-ordinates x_i $(i = 1, 2, 3)$ to describe infinitesimal deformations of an N-layer laminated elastic plate occupying the region $[0, L_1] \times [0, L_2] \times [-H/2, H/2]$ in the unstressed reference configuration. Each layer of the laminated plate is made of an isotropic material with material properties varying smoothly in the x_3 (thickness) direction only. The

vertical positions of the bottom and the top surfaces, and of the $N-1$ interfaces between the layers are denoted by $H^{(1)} = -H/2,\ H^{(2)}, \ldots, H^{(n)}, \ldots, H^{(N)},\ H^{(N+1)} = H/2$.

Equations of motion in the absence of body forces are

$$\sigma_{ij,j} = \rho \ddot{u}_i \quad (i,j = 1,2,3), \tag{1}$$

where σ_{ij} are components of the Cauchy stress tensor, ρ is the mass density and u_i are the displacement components. A comma followed by index j denotes partial differentiation with respect to the position x_j of a material particle, a repeated index implies summation over the range of the index, and a superimposed dot indicates differentiation with respect to time t.

Constitutive equations for a linear elastic isotropic material are

$$\sigma_{ij} = \lambda \varepsilon_{kk} \delta_{ij} + 2\mu \varepsilon_{ij}, \tag{2}$$

where λ and μ are the Lamé constants, ε_{ij} are components of the infinitesimal strain tensor and δ_{ij} are components of the Kronecker delta. Material properties λ, μ and ρ are assumed to be analytic functions of x_3.

The strain tensor for infinitesimal deformations is related to the displacements u_i by

$$\varepsilon_{ij} = (u_{i,j} + u_{j,i})/2. \tag{3}$$

Edges of the plate are assumed to be simply supported. That is,

$$\begin{aligned} &\sigma_{11} = 0, \quad u_2 = u_3 = 0, \quad \text{at } x_1 = 0, L_1; \\ &\sigma_{22} = 0, \quad u_1 = u_3 = 0, \quad \text{at } x_2 = 0, L_2. \end{aligned} \tag{4}$$

Boundary conditions prescribed on the top and the bottom surfaces can be either a displacement component u_j or the corresponding traction component σ_{3j} or a suitable linear combination of the two. However, typically non-zero normal and zero tangential tractions are prescribed on these two surfaces. Since the normal load can be expanded as a double Fourier series in x_1 and x_2, it suffices to consider time harmonic loads of the form

$$\begin{aligned} &\sigma_{13} = \sigma_{23} = 0, \quad \text{at } x_3 = \pm H/2, \\ &\sigma_{33}(x_1, x_2, \pm H/2) = q^{\pm} \mathrm{e}^{\mathrm{i}\omega t} \sin r x_1 \sin s x_2, \end{aligned} \tag{5}$$

where q^+ and q^- are amplitudes of the normal loads applied on the top and the bottom surfaces, respectively, ω denotes the angular frequency, $r = k\pi/L_1$, $s = m\pi/L_2$, and k and m are positive integers.

The interfaces between adjoining layers are assumed to be perfectly bonded together so that

$$[\![u_i]\!] = 0, \quad [\![\sigma_{i3}]\!] = 0, \ \text{on } x_3 = H^{(2)}, H^{(3)}, \ldots, H^{(N)}. \tag{6}$$

Here, $[\![u_i]\!]$ denotes the jump in the value of u_i across an interface.

3. Exact solution

We construct a local rectangular Cartesian co-ordinate system $x_1^{(n)}, x_2^{(n)}, x_3^{(n)}$ with local axes parallel to the global axes and the origin at the point where the global x_3-axis intersects the mid surface of the nth lamina. In the local co-ordinate system, the nth lamina occupies the region $[0, L_1] \times [0, L_2] \times [-h^{(n)}/2, h^{(n)}/2]$, where $h^{(n)} = H^{(n+1)} - H^{(n)}$.

We assume that within each layer, the Lamé constants λ, μ and the mass density ρ are analytic functions of x_3 and thus can be represented by a Taylor series expansion about its midsurface as

$$[\lambda^{(n)}, \mu^{(n)}, \rho^{(n)}] = \sum_{\alpha=0}^{\infty} [\tilde{\lambda}^{(n,\alpha)}, \tilde{\mu}^{(n,\alpha)}, \tilde{\rho}^{(n,\alpha)}] x_3^{\alpha}. \tag{7}$$

It should be noted that λ, μ and ρ are positive quantities for all x_3, and therefore $\tilde{\lambda}^{(n,0)}$, $\tilde{\mu}^{(n,0)}$ and $\tilde{\rho}^{(n,0)}$ are positive.

A solution for the displacement field in the nth layer is sought in the form

$$\begin{aligned} u_1^{(n)} &= \sum_{r,s} U_{1rs}^{(n)}(x_3) e^{i\omega t} \cos rx_1 \sin sx_2, \\ u_2^{(n)} &= \sum_{r,s} U_{2rs}^{(n)}(x_3) e^{i\omega t} \sin rx_1 \cos sx_2, \\ u_3^{(n)} &= \sum_{r,s} U_{3rs}^{(n)}(x_3) e^{i\omega t} \sin rx_1 \sin sx_2. \end{aligned} \tag{8}$$

The chosen displacement field (8) identically satisfies homogeneous boundary conditions (4) at simply supported edges. In order to simplify the notation, we henceforth drop the summation on r and s, and the subscripts r and s on $U_1^{(n)}$, $U_2^{(n)}$ and $U_3^{(n)}$. For loads given by Eq. (5) it is reasonable to assume that only one term in Eqs. (8) will be non-vanishing. Substitution for $\mathbf{u}$ from Eqs. (8) into Eq. (3), and for ε_{ij} into the constitutive equations (2) gives stresses in terms of displacements as

$$\begin{aligned} \sigma_{11}^{(n)} &= [-(\lambda^{(n)} + 2\mu^{(n)}) U_1^{(n)} r - \lambda^{(n)} U_2^{(n)} s + \lambda^{(n)} (U_3^{(n)})'] e^{i\omega t} \sin rx_1 \sin sx_2, \\ \sigma_{22}^{(n)} &= [-(\lambda^{(n)} + 2\mu^{(n)}) U_2^{(n)} s - \lambda^{(n)} U_1^{(n)} r + \lambda^{(n)} (U_3^{(n)})'] e^{i\omega t} \sin rx_1 \sin sx_2, \\ \sigma_{33}^{(n)} &= [-\lambda^{(n)} U_1^{(n)} r - \lambda^{(n)} U_2^{(n)} s + (\lambda^{(n)} + 2\mu^{(n)}) (U_3^{(n)})'] e^{i\omega t} \sin rx_1 \sin sx_2, \\ \sigma_{12}^{(n)} &= \mu^{(n)} (U_1^{(n)} s + U_2^{(n)} r) e^{i\omega t} \cos rx_1 \cos sx_2, \\ \sigma_{13}^{(n)} &= \mu^{(n)} [(U_1^{(n)})' + U_3^{(n)} r] e^{i\omega t} \cos rx_1 \sin sx_2, \\ \sigma_{23}^{(n)} &= \mu^{(n)} [(U_2^{(n)})' + U_3^{(n)} s] e^{i\omega t} \sin rx_1 \cos sx_2, \end{aligned} \tag{9}$$

where a prime denotes differentiation with respect to x_3. Stresses in Eqs. (9) are substituted into equations of motion (1) to obtain the following coupled system of second order ordinary differential equations for $U_1^{(n)}$, $U_2^{(n)}$ and $U_3^{(n)}$:

$$\begin{aligned} &(\lambda^{(n)} + 2\mu^{(n)}) U_1^{(n)} r^2 + \lambda^{(n)} U_2^{(n)} rs + \mu^{(n)} (U_1^{(n)} s^2 + U_2^{(n)} rs) - \lambda^{(n)} (U_3^{(n)})' r \\ &\quad - (\mu^{(n)})' [(U_1^{(n)})' + U_3^{(n)} r] - \mu^{(n)} [(U_1^{(n)})'' + (U_3^{(n)})' r] - \rho^{(n)} \omega^2 U_1^{(n)} = 0, \\ &(\lambda^{(n)} + 2\mu^{(n)}) U_2^{(n)} s^2 + \lambda^{(n)} U_1^{(n)} rs + \mu^{(n)} (U_2^{(n)} s^2 + U_1^{(n)} rs) - \lambda^{(n)} (U_3^{(n)})' s \\ &\quad - (\mu^{(n)})' [(U_2^{(n)})' + U_3^{(n)} s] - \mu^{(n)} [(U_2^{(n)})'' + (U_3^{(n)})' s] - \rho^{(n)} \omega^2 U_2^{(n)} = 0, \\ &\mu^{(n)} [(U_1^{(n)})' r + (U_2^{(n)})' s] + \mu^{(n)} U_3^{(n)} (r^2 + s^2) + (\lambda^{(n)})' (U_1^{(n)} r + U_2^{(n)} s) - (\lambda^{(n)} + 2\mu^{(n)}) (U_3^{(n)})'' \\ &\quad + \lambda^{(n)} [(U_1^{(n)})' r + (U_2^{(n)})' s] - [(\lambda^{(n)})' + 2(\mu^{(n)})'] (U_3^{(n)})' - \rho^{(n)} \omega^2 U_3^{(n)} = 0. \end{aligned} \tag{10}$$

We assume a power series solution for the displacement function $U_i^{(n)}(x_3)$ as

$$U_i^{(n)}(x_3) = \sum_{\beta=0}^{\infty} \tilde{U}_i^{(n,\beta)} x_3^{\beta}, \tag{11}$$

and note that $\tilde{U}_i^{(n,\beta)}$, for $\beta = 1, 2, \ldots$ have different dimensional units. For example, $\tilde{U}_i^{(n,0)}$ has units of length, $\tilde{U}_i^{(n,1)}$ is dimensionless, and $\tilde{U}_i^{(n,2)}$ has units of 1/length. Inserting the Taylor series expansion for the material properties λ, μ and ρ from Eq. (7) and the assumed power series solution for the displacements from Eq. (11) into the differential equations (10) and equating like powers of x_3 on both sides of the equation, we obtain the following coupled recurrence algebraic relations that have to be satisfied for every non-negative integer $\alpha \in [0, \infty)$:

$$\begin{aligned}
&\sum_{\beta=0}^{\alpha} \{(\tilde{\lambda}^{(n,\beta)} + 2\tilde{\mu}^{(n,\beta)})\tilde{U}_1^{(n,\alpha-\beta)} r^2 + \tilde{\lambda}^{(n,\beta)}\tilde{U}_2^{(n,\alpha-\beta)} rs + \tilde{\mu}^{(n,\beta)}(\tilde{U}_1^{(n,\alpha-\beta)} s^2 + \tilde{U}_2^{(n,\alpha-\beta)} rs) \\
&\quad - (\alpha-\beta+1)\tilde{\lambda}^{(n,\beta)}\tilde{U}_3^{(n,\alpha-\beta+1)} r - (\beta+1)\tilde{\mu}^{(n,\beta+1)}((\alpha-\beta+1)\tilde{U}_1^{(n,\alpha-\beta+1)} + \tilde{U}_3^{(n,\alpha-\beta)} r) \\
&\quad - (\alpha-\beta+1)\tilde{\mu}^{(n,\beta)}((\alpha-\beta+2)\tilde{U}_1^{(n,\alpha-\beta+2)} + \tilde{U}_3^{(n,\alpha-\beta+1)} r) - \tilde{\rho}^{(n,\beta)}\tilde{U}_1^{(n,\alpha-\beta)}\omega^2\} = 0, \\
&\sum_{\beta=0}^{\alpha} \{(\tilde{\lambda}^{(n,\beta)} + 2\tilde{\mu}^{(n,\beta)})\tilde{U}_2^{(n,\alpha-\beta)} s^2 + \tilde{\lambda}^{(n,\beta)}\tilde{U}_1^{(n,\alpha-\beta)} rs + \tilde{\mu}^{(n,\beta)}(\tilde{U}_2^{(n,\alpha-\beta)} r^2 + \tilde{U}_1^{(n,\alpha-\beta)} rs) \\
&\quad - (\alpha-\beta+1)\tilde{\lambda}^{(n,\beta)}\tilde{U}_3^{(n,\alpha-\beta+1)} s - (\beta+1)\tilde{\mu}^{(n,\beta+1)}((\alpha-\beta+1)\tilde{U}_2^{(n,\alpha-\beta+1)} + \tilde{U}_3^{(n,\alpha-\beta)} s) \\
&\quad - (\alpha-\beta+1)\tilde{\mu}^{(n,\beta)}((\alpha-\beta+2)\tilde{U}_2^{(n,\alpha-\beta+2)} + \tilde{U}_3^{(n,\alpha-\beta+1)} s) - \tilde{\rho}^{(n,\beta)}\tilde{U}_2^{(n,\alpha-\beta)}\omega^2\} = 0, \\
&\sum_{\beta=0}^{\alpha} \{\tilde{\mu}^{(n,\beta)}(\alpha-\beta+1)(\tilde{U}_1^{(n,\alpha-\beta+1)} r + \tilde{U}_2^{(n,\alpha-\beta+1)} s) + \tilde{\mu}^{(n,\beta)}\tilde{U}_3^{(n,\alpha-\beta)}(r^2+s^2) \\
&\quad + (\alpha-\beta+1)\tilde{\lambda}^{(n,\beta)}(\tilde{U}_1^{(n,\alpha-\beta+1)} r + \tilde{U}_2^{(n,\alpha-\beta+1)} s) + (\beta+1)\tilde{\lambda}^{(n,\beta+1)}(\tilde{U}_1^{(n,\alpha-\beta)} r + \tilde{U}_2^{(n,\alpha-\beta)} s) \\
&\quad - (\alpha-\beta+2)(\alpha-\beta+1)(\tilde{\lambda}^{(n,\beta)} + 2\tilde{\mu}^{(n,\beta)})\tilde{U}_3^{(n,\alpha-\beta+2)} \\
&\quad - (\beta+1)(\alpha-\beta+1)(\tilde{\lambda}^{(n,\beta+1)} + 2\tilde{\mu}^{(n,\beta+1)})\tilde{U}_3^{(n,\alpha-\beta+1)} - \tilde{\rho}^{(n,\beta)}\tilde{U}_3^{(n,\alpha-\beta)}\omega^2\} = 0.
\end{aligned} \tag{12}$$

3.1. Natural frequencies

The simply supported plate is in a state of free vibration if no loads are applied on its top and bottom surfaces, i.e., $q^+ = q^- = 0$. The recurrence relations (12) are evaluated successively for $\alpha = 0, 1, \ldots,$ to obtain $\tilde{U}_1^{(n,\alpha+2)}$, $\tilde{U}_2^{(n,\alpha+2)}$ and $\tilde{U}_3^{(n,\alpha+2)}$ in terms of six arbitrary constants $\tilde{U}_1^{(n,0)}$, $\tilde{U}_1^{(n,1)}$, $\tilde{U}_2^{(n,0)}$, $\tilde{U}_2^{(n,1)}$, $\tilde{U}_3^{(n,0)}$, $\tilde{U}_3^{(n,1)}$ and the angular frequency ω as

$$\tilde{U}_i^{(n,\alpha+2)} = \sum_{j=1}^{3} [a_{ij}^{(n,\alpha+2)}(\omega)\tilde{U}_j^{(n,0)} + b_{ij}^{(n,\alpha+2)}(\omega)\tilde{U}_j^{(n,1)}]. \tag{13}$$

Here, $a_{ij}^{(n,\alpha+2)}(\omega)$ and $b_{ij}^{(n,\alpha+2)}(\omega)$ are known polynomials in ω. The degree of each of the polynomials increases as more terms are retained in the series expansion (11). There are six

arbitrary constants, namely $\tilde{U}_j^{(n,0)}$ and $\tilde{U}_j^{(n,1)}$, for each layer, resulting in a total of $6N$ unknowns for an N-layer plate.

Substitution of Eq. (13) into Eq. (11) and the result into Eqs. (9) gives stresses in terms of the arbitrary constants and ω. The satisfaction of the interface continuity conditions (6) between adjoining layers results in the following homogeneous matrix equation:

$$\mathbf{G}(\omega)\mathbf{W} = \mathbf{0},$$

where $\mathbf{G}(\omega)$ is a $6N \times 6N$ matrix whose elements are polynomials of ω and $\mathbf{W}$ is a vector of length $6N$ consisting of the unknowns $\tilde{U}_j^{(n,0)}$ and $\tilde{U}_j^{(n,1)}$. A non-trivial solution for $\mathbf{W}$ is obtained by setting the determinant $|\mathbf{G}(\omega)|$ equal to zero. The resulting polynomial equation is solved to obtain a set of eigenvalues that are arranged in increasing order as $\{\omega_{k,m}^{(1)}, \omega_{k,m}^{(2)}, \omega_{k,m}^{(3)}, \omega_{k,m}^{(4)}, \ldots\}$ which are the natural frequencies (eigenvalues) of the plate corresponding to integers k and m defining the in-plane mode shape. The eigenvector $\mathbf{W}^{(j)}$ associated with the eigenvalue $\omega_{k,m}^{(j)}$ is determined from the nullspace of $\mathbf{G}(\omega_{k,m}^{(j)})$ and is normalized by Eqs. (27).

3.2. Forced vibrations

The plate is in a state of forced vibration if either q^+ or q^-, or both are non-zero. The recurrence relations (12) are evaluated successively for $\alpha = 0, 1, \ldots$, to obtain $\tilde{U}_1^{(n,\alpha+2)}$, $\tilde{U}_2^{(n,\alpha+2)}$ and $\tilde{U}_3^{(n,\alpha+2)}$ in terms of arbitrary constants $\tilde{U}_1^{(n,0)}$, $\tilde{U}_1^{(n,1)}$, $\tilde{U}_2^{(n,0)}$, $\tilde{U}_2^{(n,1)}$, $\tilde{U}_3^{(n,0)}$ and $\tilde{U}_3^{(n,1)}$. Thus, there are six unknown constants for each layer, resulting in a total of $6N$ unknowns for an N-layer plate. The constants are determined by satisfying boundary conditions (5) on the top and the bottom surfaces of the plate and continuity conditions (6) at the interfaces between adjoining layers. This yields six conditions for the top and the bottom surfaces and six conditions at each of the $N-1$ interfaces. The resulting system of $6N$ linear algebraic equations for the $6N$ unknowns is readily solved to obtain displacements and stresses for the entire plate.

4. Plate theories

The material in this section can be derived from Refs. [40–47], and is similar to that summarized in Ref. [10]. It is included for the sake of completeness. For a laminated plate, it will require modifications to enforce continuity of displacements and normal tractions at the interfaces between adjoining layers. The displacement field for the CPT [40], the FSDT [41,42] and the TSDT [43] can be written as

$$u_\alpha(x_i,t) = u_\alpha^\circ(x_\beta,t) - x_3 u_{3,\alpha}^\circ + g(x_3)\varphi_\alpha(x_\beta,t), \quad u_3(x_i,t) = u_3^\circ(x_\beta,t), \quad \alpha,\beta = 1,2, \tag{14}$$

where u_α°, u_3° and φ_γ are independent of x_3 and the function $g(x_3) = 0$ for the CPT, $g(x_3) = x_3$ for the FSDT and $g(x_3) = x_3(1 - 4x_3^2/3h^2)$ for the TSDT. In this section, Latin indices range from 1 to 3 and Greek indices from 1 to 2. Functions $\boldsymbol{u}^\circ$ give displacements of a point on the midsurface of the plate and for the FSDT $(\varphi_1 - u_{3,1}^\circ)$ and $(-\varphi_2 + u_{3,2}^\circ)$ are respectively rotations of the transverse normal to the midsurface about the x_2- and x_1-axis.

For infinitesimal deformations of a functionally graded plate subjected to an arbitrary distributed normal load $p(x_\alpha)$ on its major surfaces, the field equations are

$$\begin{aligned} &N_{\alpha\beta,\beta} = I_0\ddot{u}_\alpha^\circ - I_4\ddot{u}_{3,\alpha}^\circ + I_5\ddot{\varphi}_\alpha,\\ &M_{\alpha\beta,\alpha\beta} + p = I_0\ddot{u}_3^\circ - I_1\ddot{u}_{3,\alpha\alpha}^\circ + I_2\ddot{\varphi}_{\alpha,\alpha} + I_4\ddot{u}_{\alpha,\alpha},\\ &P_{\alpha\beta,\beta} - \mathscr{K}R_\alpha = I_3\ddot{\varphi}_\alpha - I_2\ddot{u}_{3,\alpha}^\circ + I_5\ddot{u}_\alpha, \end{aligned} \tag{15}$$

where the stress resultants and moments of inertia are defined as

$$[N_{\alpha\beta}, M_{\alpha\beta}, P_{\alpha\beta}] = \int_{-H/2}^{H/2} \sigma_{\alpha\beta}[1, x_3, g]\,\mathrm{d}x_3, \quad R_\alpha = \int_{-H/2}^{H/2} \sigma_{\alpha 3} g_{,3}\,\mathrm{d}x_3,$$

$$\begin{bmatrix} I_0 & I_4 & I_5 \\ I_4 & I_1 & I_2 \\ I_5 & I_2 & I_3 \end{bmatrix} = \int_{-H/2}^{H/2} \begin{bmatrix} 1 & x_3 & g \\ x_3 & x_3^2 & x_3 g \\ g & x_3 g & g^2 \end{bmatrix} \rho\,\mathrm{d}x_3, \tag{16}$$

and constant $\mathscr{K}$ is the shear correction factor used only for the FSDT. We set $\mathscr{K} = 5/6 = 0.83333$ although this value was proposed by Reissner for a homogeneous plate. Mindlin [42] showed that for the FSDT to predict correctly the first antisymmetric mode of thickness-shear vibration, defined by the displacement field $u_j = u(x_3)\mathrm{e}^{\mathrm{i}\omega t}\delta_{j1}$ in a homogeneous isotropic plate, $\mathscr{K}^2 = \pi^2/12 = 0.823129$. We note that in Ref. [10], the thickness-shear vibration refers to the mode associated with the rotational angles of a normal to the midsurface of the plate.

The transverse normal stress σ_{33} is assumed to be negligible and has been set equal to zero in each one of the three plate theories. Setting $\sigma_{33} = 0$ in Eq. (2), solving the resulting equation for ε_{33} and substituting for ε_{33} into Eq. (2) gives

$$\sigma_{\alpha\beta} = \frac{2\nu\mu}{1-\nu}\varepsilon_{\omega\omega}\delta_{\alpha\beta} + 2\mu\varepsilon_{\alpha\beta}, \quad \sigma_{\alpha 3} = 2\mu\varepsilon_{\alpha 3}, \tag{17}$$

where ν is the Poisson ratio. For a functionally graded plate the material properties are assumed to vary in the thickness direction only, that is, $\nu = \nu(x_3), \mu = \mu(x_3)$.

The boundary conditions for a simply supported plate are

$$\begin{aligned} &N_{11} = 0,\ M_{11} = 0,\ P_{11} = 0,\ u_3^\circ = 0,\ u_2^\circ = 0,\ \varphi_2 - u_{3,2}^\circ = 0 \quad \text{at } x_1 = 0, L_1,\\ &N_{22} = 0,\ M_{22} = 0,\ P_{22} = 0,\ u_3^\circ = 0,\ u_1^\circ = 0,\ \varphi_1 - u_{3,1}^\circ = 0 \quad \text{at } x_2 = 0, L_2. \end{aligned} \tag{18}$$

For loads given by Eq. (7) or for free vibrations, a solution of partial differential equations (15) can be obtained by choosing displacements and rotations as

$$\begin{aligned} &[u_1^\circ, \varphi_1] = [S_1, S_2]\mathrm{e}^{\mathrm{i}\omega t}\cos rx_1 \sin sx_2,\\ &[u_2^\circ,\ \varphi_2] = [S_3, S_4]\mathrm{e}^{\mathrm{i}\omega t}\sin rx_1 \cos sx_2,\\ &u_3^\circ = S_5\mathrm{e}^{\mathrm{i}\omega t}\sin rx_1 \sin sx_2. \end{aligned} \tag{19}$$

For arbitrary values of $S_1, S_2, \ldots, S_5$, the assumed fields (19) satisfy boundary conditions (18) identically. Boundary conditions (4) of the 3-D elasticity theory imply those in Eqs. (18) and

require that $\varphi_2 = 0$ at $x_1 = 0, L_1$, and $\varphi_1 = 0$ at $x_2 = 0, L_2$. For free vibrations of a plate, $p(x_\alpha) = 0$. Substitution from Eqs. (19), (14) and (3) into Eqs. $(16)_{3,4}$ and the result into Eqs. (15) yields five linear homogeneous coupled equations in the five unknowns $S_1, S_2, \ldots, S_5$. In order for these equations to have a non-trivial solution, the determinant of the coefficient matrix must be zero. We thus obtain a polynomial equation for the determination of the frequency ω. The corresponding eigenvector is found from any four of the five equations for $S_1, S_2, \ldots, S_5$ and is normalized by Eqs. (27).

The transverse shear stresses σ_{13} and σ_{23} are obtained from the in-plane stresses σ_{11}, σ_{22} and σ_{12} by integrating the 3-D equations of motion in the thickness direction. That is,

$$\sigma_{j3} = \int_{-H/2}^{x_3} (\rho \ddot{u}_j - \sigma_{j\beta,\beta}) \, \mathrm{d}x_3, \quad \beta = 1, 2. \tag{20}$$

The transverse normal stress σ_{33} is determined, also using Eq. (20), after the transverse shear stresses have been found.

5. Effective moduli of two-phase composites

Consider a functionally graded composite material fabricated by mixing two distinct material phases, for example, a metal and a ceramic. Often, precise information about the size, the shape and the distribution of particles may not be available and the effective elastic moduli of the graded composite must be evaluated based only on the volume fraction distribution and the approximate shape of the dispersed phase. Several micromechanics models have been developed over the years to infer the effective properties of macroscopically homogeneous composite materials. We summarize below the Mori–Tanaka and the self-consistent methods for estimating the effective properties, and use them to analyze functionally graded plates. In each case, the macroscopic response of the 2-phase composite made of isotropic constituents is assumed to be isotropic.

5.1. The Mori–Tanaka estimate

The Mori–Tanaka scheme [32,33] for estimating the effective moduli is applicable to regions of the graded microstructure which have a well-defined continuous matrix and a discontinuous particulate phase as depicted in Fig. 1(a). It takes into account the interaction of the elastic fields among neighboring inclusions. It is assumed that the matrix phase, denoted by the subscript 1, is reinforced by spherical particles of a particulate phase, denoted by the subscript 2. In this notation, K_1, μ_1 and V_1 denote respectively the bulk modulus, the shear modulus and the volume fraction of the matrix phase; K_2, μ_2 and V_2 denote the corresponding material properties and the volume fraction of the particulate phase. It should be noted that $V_1 + V_2 = 1$, the Lamé constant λ is related to the bulk and the shear moduli by $\lambda = K - 2\mu/3$. The effective mass density at a point is given by the "rule of mixture":

$$\rho = \rho_1 V_1 + \rho_2 V_2. \tag{21}$$

The effective local bulk modulus K and the shear modulus μ obtained by the Mori–Tanaka scheme for a random distribution of isotropic particles in an isotropic matrix

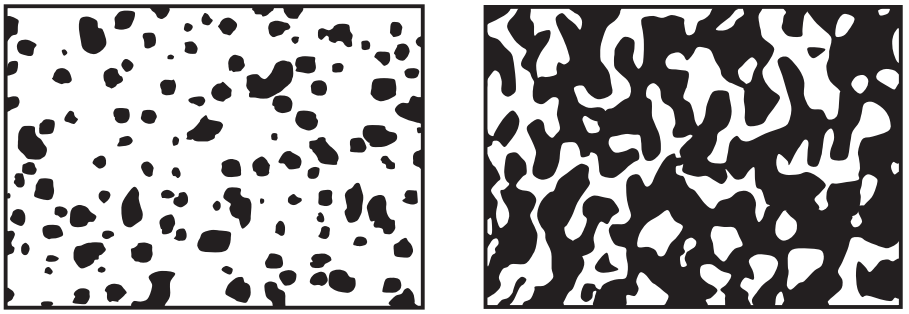

(a) (b)

Fig. 1. Two-phase material with (a) particulate microstructure and (b) skeletal microstructure.

are given by

$$\frac{K-K_1}{K_2-K_1}=V_2\Big/\left(1+(1-V_2)\frac{K_2-K_1}{K_1+(4/3)\mu_1}\right),$$

$$\frac{\mu-\mu_1}{\mu_2-\mu_1}=V_2\Big/\left(1+(1-V_2)\frac{\mu_2-\mu_1}{\mu_1+f_1}\right), \tag{22}$$

where $f_1=\mu_1(9K_1+8\mu_1)/6(K_1+2\mu_1)$.

5.2. Self-consistent estimate

The self-consistent method [34] assumes that each reinforcement inclusion is embedded in a continuum material whose effective properties are those of the composite. This method does not distinguish between matrix and reinforcement phases and the same overall moduli are predicted in another composite in which the roles of the phases are interchanged. This makes it particularly suitable for determining the effective moduli in those regions which have an interconnected skeletal microstructure as depicted in Fig. 1(b). The locally effective elastic moduli by the self-consistent method are given by

$$\begin{aligned}\delta/K&=V_1/(K-K_2)+V_2/(K-K_1),\\ \eta/\mu&=V_1/(\mu-\mu_2)+V_2/(\mu-\mu_1),\end{aligned} \tag{23}$$

where $\delta=3-5\eta=K/(K+4\mu/3)$. The first equation (23) when solved for K in terms of μ gives

$$K=1/(V_1/(K_1+4\mu/3)+V_2/(K_2+4\mu/3))-4\mu/3, \tag{24}$$

and μ is obtained by solving the following quartic equation:

$$[V_1K_1/(K_1+4\mu/3)+V_2K_2/(K_2+4\mu/3)]+5[V_1\mu_2/(\mu-\mu_2)+V_2\mu_1/(\mu-\mu_1)]+2=0. \tag{25}$$

Since the quartic equation (25) has to be solved to find the shear modulus μ, it is easier to use the Mori–Tanaka method than the self-consistent scheme.

6. Results and discussion

Since it is common in high temperature applications to employ a ceramic top layer as a thermal barrier to a metallic structure, we choose the constituent materials of the functionally graded plate to be aluminum and zirconia with material properties:

$$\text{Al}: E_m = 70 \text{ GPa}, \quad \nu_m = 0.3, \quad \rho_m = 2702 \text{ kg/m}^3,$$

$$\text{ZrO}_2: E_c = 200 \text{ GPa}, \quad \nu_c = 0.3, \quad \rho_c = 5700 \text{ kg/m}^3.$$

Recall that the bulk modulus and the shear modulus are related to Young's modulus E and the Poisson ratio ν by $K = E/3(1-2\nu)$ and $\mu = E/2(1+\nu)$. We assume that the volume fraction of the ceramic phase is given by the power-law function

$$V_c = V_c^- + (V_c^+ - V_c^-)\left(\frac{1}{2} + \frac{x_3}{H}\right)^p. \tag{26}$$

Here, V_c^+ and V_c^- are, respectively, the volume fractions of the ceramic phase on the top and the bottom surfaces of the plate, and p is a parameter that dictates the volume fraction profile through the thickness. Cheng and Batra [18] have also used a similar power-law function for the volume fraction, except that they have assumed $V_c^+ = 1$ and $V_c^- = 0$.

The integers k and m in Eqs. (8) define the in-plane mode shape. Corresponding to each in-plane mode shape, there are an infinite number of natural frequencies (eigenvalues) $\omega_{k,m}^{(j)}$, each one of them representing a different *thickness-mode*. The first eigenvalue $\omega_{k,m}^{(1)}$ is generally referred to the *flexural mode eigenvalue*. In the tables and figures to follow, frequencies, displacements or mode shapes and stresses are non-dimensionalized as

$$\bar{\omega} = \frac{\omega L_1^2}{H}\sqrt{\frac{\rho_m}{E_m}}, \quad \bar{u}_1(x_3) = \frac{u_1(0, L_2/2m, x_3)L_1}{u_3(L_1/2k, L_2/2m, 0)H},$$

$$\bar{\sigma}_{11}(x_3) = \frac{\sigma_{11}(L_1/2k, L_2/2m, x_3)L_1^2}{10E_m u_3(L_1/2k, L_2/2m, 0)H}, \quad \bar{\sigma}_{12}(x_3) = \frac{\sigma_{11}(0, 0, x_3)L_1^2}{10E_m u_3(L_1/2k, L_2/2m, 0)H},$$

$$\bar{\sigma}_{13}(x_3) = \frac{\sigma_{13}(0, L_2/2m, x_3)L_1^3}{10E_m u_3(L_1/2k, L_2/2m, 0)H^2}, \quad \bar{\sigma}_{33}(x_3) = \frac{\sigma_{33}(L_1/2k, L_2/2m, x_3)L_1^4}{E_m u_3(L_1/2k, L_2/2m, 0)H^3}. \tag{27}$$

6.1. Validation of the approach

The solution procedure is validated by comparing the natural frequencies for a simply supported square homogeneous aluminum (Al) plate with those of Srinivas et al. [13]. The first nine thickness-mode eigenvalues corresponding to $k = m = 1$, using 50 terms in the series expansion (11) for the displacements, are given in Table 1. Batra and Aimmanee [48] have reported that one should also study cases for which either k or m equals zero. When either k or m equals 0, $u_3 \equiv 0$, the dilatation equals zero and the lowest frequency of in-plane pure distortional modes for a thick plate is smaller than the second or the third lowest frequency of the flexural mode. These modes of vibration were missed by Srinivas et al. [14] and by subsequent researchers. An exception is the work of Soldatos and Hadjigeorgiou [49] who gave the missing frequencies but

Table 1
Comparison of exact natural frequencies with those given by Srinivas et al. [13] for a homogeneous aluminum square plate with 50 terms in the series solution

Theory	$\bar{\omega}_{1,1}^{(1)a}$	$\bar{\omega}_{1,1}^{(2)b}$	$\bar{\omega}_{1,1}^{(3)b}$	$\bar{\omega}_{1,1}^{(4)a}$	$\bar{\omega}_{1,1}^{(5)a}$	$\bar{\omega}_{1,1}^{(6)b}$	$\bar{\omega}_{1,1}^{(7)b}$	$\bar{\omega}_{1,1}^{(8)b}$	$\bar{\omega}_{1,1}^{(9)a}$
$L_1/H = \sqrt{10}$									
Present analysis	4.6582	8.7132	14.463	21.343	24.830	33.982	39.929	44.544	58.411
Srinivas et al. [13]	4.6582	8.7134	14.462	21.343	24.830	33.982	39.929	44.544	58.410
CPT	5.5354	8.7132	14.728	—	—	—	—	—	—
FSDT	4.6181	8.7132	14.728	21.460	25.367	—	—	—	—
TSDT	4.4291	8.7132	14.728	21.769	26.268	—	—	—	—
$L_1/H = 10$									
Present analysis	5.7769	27.554	46.503	196.77	201.34	357.42	390.64	399.77	584.34
Srinivas et al. [13]	5.7769	27.554	46.502	196.77	201.34	357.42	390.64	399.77	584.35
CPT	5.9248	27.554	46.574	—	—	—	—	—	—
FSDT	5.7693	27.554	46.574	198.04	203.05	—	—	—	—
TSDT	5.7317	27.554	46.574	197.35	203.16	—	—	—	—

[a] Antisymmetric thickness mode.
[b] Symmetric thickness mode.

not the mode shapes. The present analysis correctly predicts these frequencies of pure distortional modes of vibration. A glance at the values in Table 1 reveals that our results are in excellent agreement with those of Srinivas et al. [13]. We have also listed in Table 1 the natural frequencies computed from the three plate theories.

For $L_1/H = \sqrt{10}$ and 10, the FSDT and the TSDT predict the first flexural frequency accurately; however, the CPT does so only for $L_1/H = 10$. This is to be expected since transverse shear deformations are neglected in the CPT but are considered in the other two plate theories. The through-the-thickness variation of the exact displacements and stresses corresponding to the first nine thickness modes are plotted in Fig. 2 for a homogeneous thick Al plate. Usually it is assumed that $S_1 = S_3 = 0$ in the CPT, FSDT and the TSDT. Therefore, for the three plate theories, Srinivas et al. [14] did not include frequencies corresponding to the second and the third thickness-modes shown in Fig. 2. We, however, have *not* assumed $S_1 = S_3 = 0$ for any of the three plate theories. The CPT theory solutions for the symmetric mode $\bar{\omega} = \bar{\omega}_{1,1}^{(2)}$ corresponds to $S_1 = -S_3$ and $S_5 = 0$, while the symmetric thickness-mode $\bar{\omega} = \bar{\omega}_{1,1}^{(3)}$ corresponds to $S_1 = S_3$ and $S_5 = 0$. Although the CPT results for the first two symmetric mode eigenvalues are close to the corresponding exact values (see Table 1), the CPT is inaccurate for mode $\bar{\omega}_{1,1}^{(3)}$ since it gives zero transverse shear stress σ_{13} and zero transverse normal stress σ_{33}.

Batra and Vidoli [27] have proposed a higher order shear and normal deformable plate theory that accounts for deformations symmetric about the midsurface of a homogeneous plate. Batra et al. [50] used it to study propagation of plane waves in, and vibrations of, an orthotropic homogeneous plate. Qian et al. [26,51,52] have used the plate theory for analyzing static and dynamic deformations of thick plates under different edge conditions. Computed results have been found to agree very well with those obtained from the 3-D analysis of the corresponding problems.

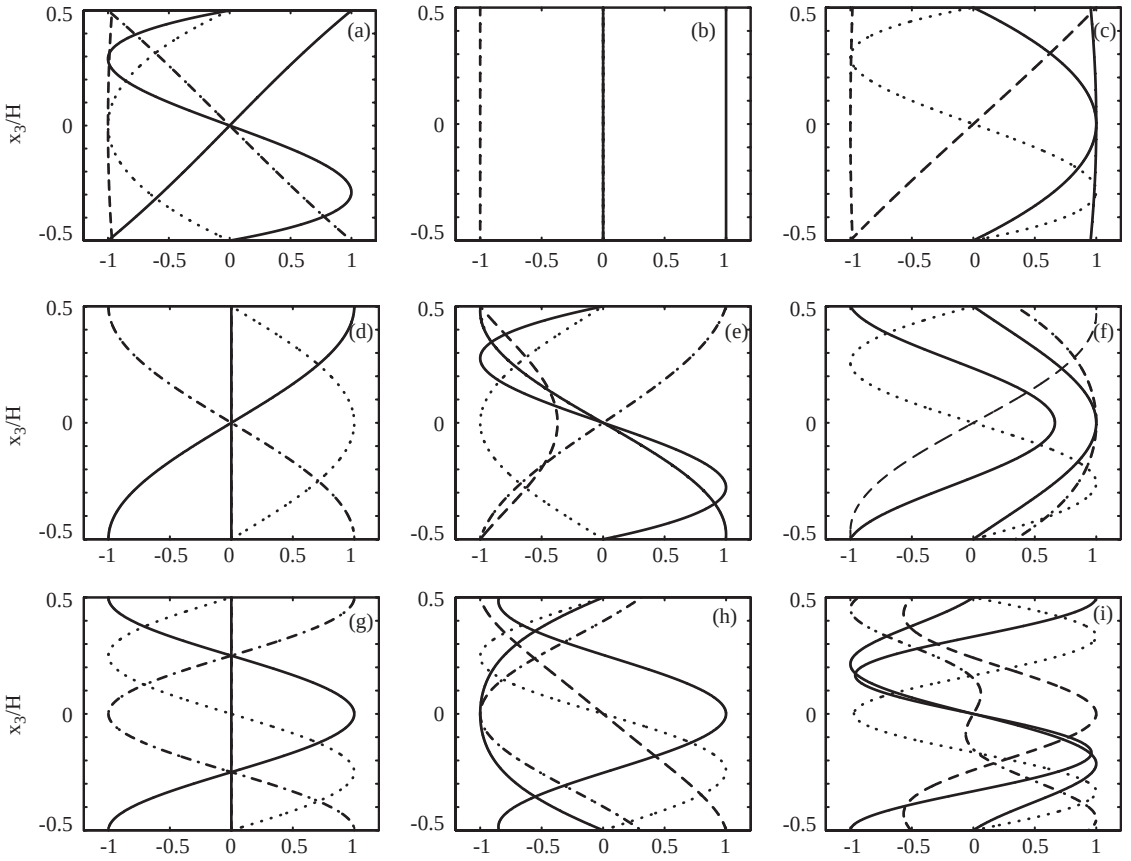

Fig. 2. The first nine through-the-thickness displacement and stress mode shapes for a homogeneous Al plate, $L_1/H = 5$: ——, $u_1(0, L_2/2, x_3)/\text{Max}|u_1(0, L_2/2, x_3)|$; – – –, $u_3(L_1/2, L_2/2, x_3)/\text{Max}|u_3(L_1/2, L_2/2, x_3)|$; – · – · –, $\sigma_{11}(L_1/2, L_2/2, x_3)/\text{Max}|\sigma_{11}(L_1/2, L_2/2, x_3)|$; ·····, $\sigma_{13}(0, L_2/2, x_3)/\text{Max}|\sigma_{13}(0, L_2/2, x_3)|$; ——, $\sigma_{33}(L_1/2, L_2/2, x_3)/\text{Max}|\sigma_{33}(L_1/2, L_2/2, x_3)|$. (a) $\bar{\omega} = \bar{\omega}^{(1)}_{1,1} = 5.3036$, (b) $\bar{\omega} = \bar{\omega}^{(2)}_{1,1} = 13.777$, (c) $\bar{\omega} = \bar{\omega}^{(3)}_{1,1} = 23.136$, (d) $\bar{\omega} = \bar{\omega}^{(4)}_{1,1} = 50.619$, (e) $\bar{\omega} = \bar{\omega}^{(5)}_{1,1} = 54.727$, (f) $\bar{\omega} = \bar{\omega}^{(6)}_{1,1} = 86.840$, (g) $\bar{\omega} = \bar{\omega}^{(7)}_{1,1} = 98.386$, (h) $\bar{\omega} = \bar{\omega}^{(8)}_{1,1} = 104.75$, (i) $\bar{\omega} = \bar{\omega}^{(9)}_{1,1} = 146.01$.

6.2. Functionally graded plate with a uniform microstructure

We consider a simply supported metal–ceramic graded square plate ($L_2 = L_1$) with uniform microstructure through the entire thickness of the plate and employ either the Mori–Tanaka or the self-consistent scheme to obtain the effective properties. We use the label MT_m to denote the Mori–Tanaka method with metal as the matrix phase, MT_c to denote the Mori–Tanaka method with ceramic as the matrix phase and SC to denote the self-consistent scheme. For example, in the MT_m method, $P_1 = P_m$ and $P_2 = P_c$, where P stands for either the volume fraction or a material property. Through-the-thickness variation of the volume fraction and the density for different power-law exponents p are depicted in Fig. 3(a) and (b). The variation of Young's modulus and the shear modulus corresponding to the three homogenization schemes for $p = 3$ is shown in Figs. 3(c) and (d). Recalling that $\nu_m = \nu_c = 0.3$, the Poisson ratio for the homogenized medium varies between 0.294 and 0.30 for $0 \leqslant V_c \leqslant 1$.

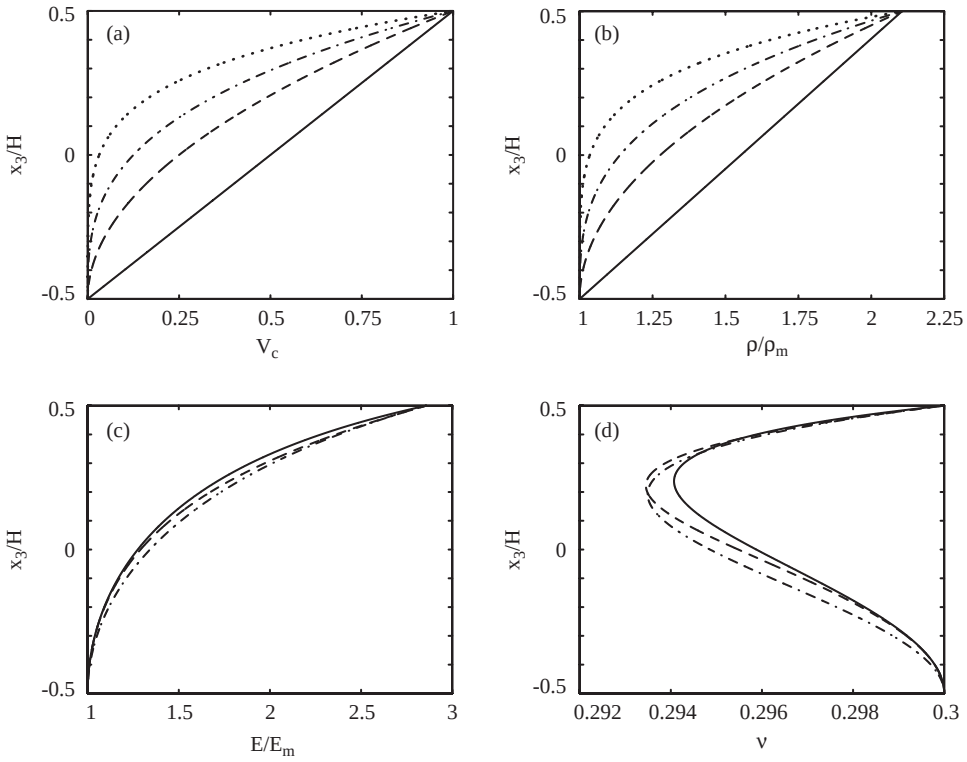

Fig. 3. Through-the-thickness distribution of the (a) ceramic volume fraction and (b) the density: ——, $p = 1$; – – –, $p = 2$; – · – · –, $p = 3$; ⋯⋯, $p = 5$. Through-the-thickness distribution of (c) Young's modulus and (d) the Poisson ratio for $p = 3$:——, MT_m; – – –, SC; – · – · –, MT_c.

The effect of truncation of series (11) on the solution is investigated for a functionally graded thick plate with $L_1/H = 5, p = 2$, $V_2^- = 0$ and $V_2^+ = 1$. The effective properties are obtained using the MT_m averaging scheme. Computed values of the natural frequency, and of normalized displacements and stresses, listed in Table 2, show that the normalized values have converged to five significant digits by retaining 50 terms, while good accuracy can be obtained by using 25 terms.

All results in the tables and plots to follow are computed by using 50 terms in series (11). With k and m set equal to 1, the first nine thickness modes for a functionally graded Al/ZrO_2 plate are shown in Fig. 4 for comparison with the thickness modes of a homogeneous aluminum plate depicted in Fig. 2; these are not the nine lowest frequencies of the Al/ZrO_2 plate which are given in Ref. [26]. Unlike the homogeneous plate, the displacements and stresses in the graded plate are no longer symmetric or antisymmetric about the mid-plane. This is because, in general, material properties for a graded plate are not symmetric about the mid-plane and their stretching and bending deformation modes are coupled.

The exact flexural natural frequencies for different modes corresponding to different values of k and m are compared with the CPT, the FSDT and the TSDT results in Fig. 5 for

Table 2
Convergence study for a square Al/ZrO_2 functionally graded thick plate

Number of terms in series	$\bar{\omega}_{1,1}^{(j)}$	$\bar{u}_1(\frac{H}{2})$	$\bar{\sigma}_{11}(\frac{H}{2})$	$\bar{\sigma}_{13}(0)$	$\bar{\sigma}_{33}(0)$
$j=1$					
10	5.1862	−1.0112	1.2886	0.82245	1.3516
25	5.1915	−1.0099	1.2950	0.82354	1.3597
50	5.1915	−1.0099	1.2950	0.82354	1.3597
$j=5$					
10	36.975	24.333	−31.104	89.371	313.60
25	36.979	24.317	−31.181	89.368	306.42
50	36.979	24.317	−31.181	89.368	306.42
$j=9$					
10	85.448	0.55356	−9.4264	−76.676	731.83
25	95.336	6.4351	−8.2516	−59.676	−186.86
50	95.336	6.4350	−8.2515	−59.676	−186.86

Effective material properties are estimated by the MT_m scheme and $L_1/H=5$, $p=2$, $V_2^-=0$, $V_2^+=1$.

length-to-thickness ratio, L_1/H, ranging from 2 to 40. The FSDT solution is in excellent agreement with the exact solution even for thick plates with $L_1/H<10$, but the CPT solution exhibits significant errors for thick and moderately thick plates. The curve for the FSDT solution essentially overlaps that for the exact solution. For each one of the four flexural frequencies and different aspect ratios of the plate, the TSDT solution exhibits larger deviations from the exact solution than that for the FSDT solution. For a fixed length-to-thickness ratio, the error in the flexural eigenvalue obtained from the CPT becomes larger as k and m increase, i.e., the error increases as the in-plane wavelengths decrease. For $(k,m)=(1,1)$, Fig. 6 exhibits plots of the normalized axial displacement and stresses versus the length-to-thickness ratio. As expected, errors in the solutions obtained from the plate theories increase as the length-to-thickness ratio decreases. Among the three plate theories considered here, the TSDT gives the most accurate results for $\bar{u}_1$ and $\bar{\sigma}_{11}$ and the FSDT gives better results for $\bar{\sigma}_{13}$ and $\bar{\sigma}_{33}$.

The through-the-thickness variations of displacements and stresses for a thick plate ($L_1/H=4$) are depicted in Fig. 7 corresponding to the eigenvalues of four different flexural mode shapes. The longitudinal displacement $\bar{u}_1$ that has an affine variation in the thickness direction for small values of k and m becomes non-linear as k and m increase. Although the strains are almost affine, the longitudinal stress $\bar{\sigma}_{11}$ is not a linear function of the thickness co-ordinate since the elastic moduli are functions of x_3. The transverse shear stress $\bar{\sigma}_{13}$ attains its maximum value at a point in the upper half of the plate.

The variations of the non-dimensional flexural frequency $\bar{\omega}_{1,1}^{(1)}$ and the corresponding displacements and stresses with the ceramic volume fraction on the top surface are depicted in Fig. 8. The natural frequency from the FSDT is in good agreement with the exact solution for all ceramic volume fractions. As is evident from these plots, all three plate theories successfully capture the qualitative behavior of the results and the percentage errors remain unchanged for

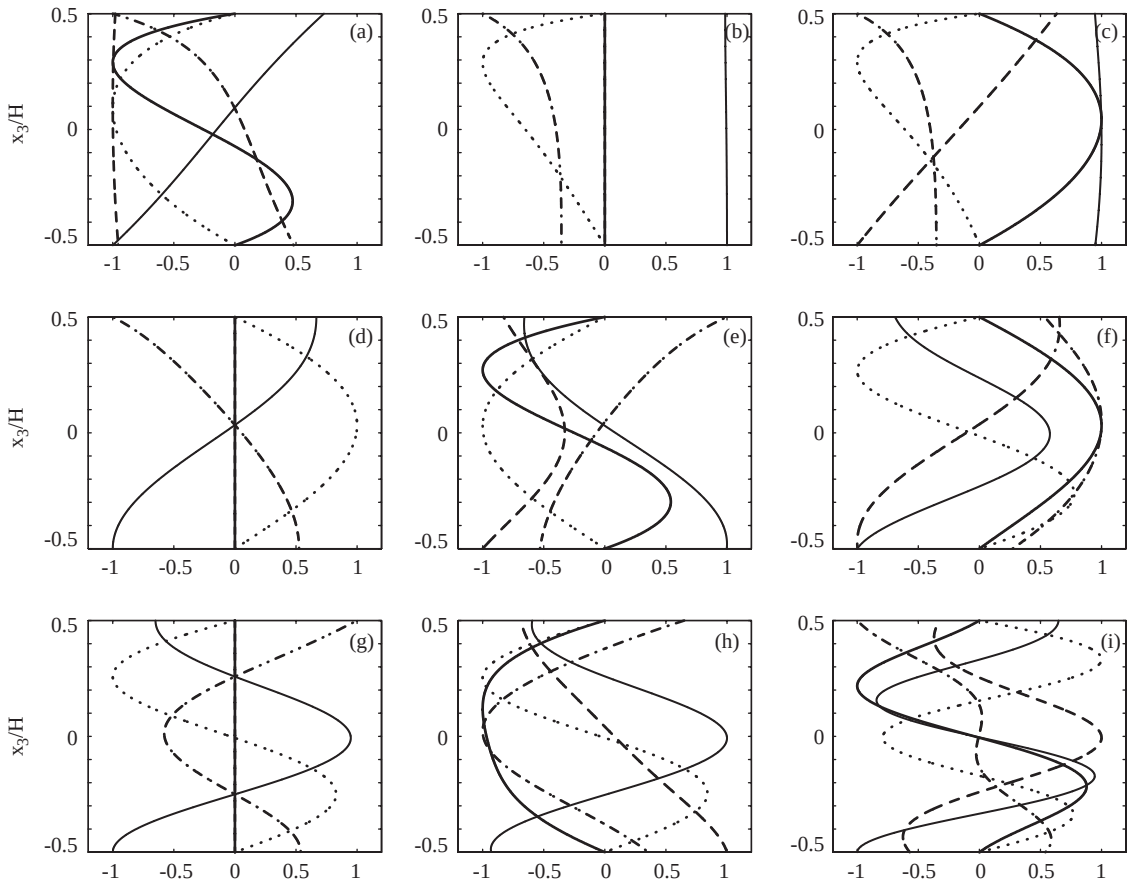

Fig. 4. The first nine through-the-thickness displacement and stress mode shapes for a Al/ZrO_2 graded thick plate, MT_m homogenization scheme, $V_c^- = 0$, $V_c^+ = 1$, $p = 3$, $L_1/H = 5$: ——, $u_1(0, L_2/2, x_3)/\text{Max}|u_1(0, L_2/2, x_3)|$; – – –, $u_3(L_1/2, L_2/2, x_3)/\text{Max}|u_3(L_1/2, L_2/2, x_3)|$; – · – · –, $\sigma_{11}(L_1/2, L_2/2, x_3)/\text{Max}|\sigma_{11}(L_1/2, L_2/2, x_3)|$; ⋯⋯, $\sigma_{13}(0, L_2/2, x_3)/\text{Max}|\sigma_{13}(0, L_2/2, x_3)|$; ——, $\sigma_{33}(L_1/2, L_2/2, x_3)/\text{Max}|\sigma_{33}(L_1/2, L_2/2, x_3)|$. (a) $\bar{\omega} = \bar{\omega}_{1,1}^{(1)}$, (b) $\bar{\omega} = \bar{\omega}_{1,1}^{(2)}$, (c) $\bar{\omega} = \bar{\omega}_{1,1}^{(3)}$, (d) $\bar{\omega} = \bar{\omega}_{1,1}^{(4)}$, (e) $\bar{\omega} = \bar{\omega}_{1,1}^{(5)}$, (f) $\bar{\omega} = \bar{\omega}_{1,1}^{(6)}$, (g) $\bar{\omega} = \bar{\omega}_{1,1}^{(7)}$, (h) $\bar{\omega} = \bar{\omega}_{1,1}^{(8)}$, (i) $\bar{\omega} = \bar{\omega}_{1,1}^{(9)}$.

different ceramic volume fractions. Fig. 9 compares the exact non-dimensional flexural frequency, displacements and stresses versus the power-law index p in Eq. (26) with results obtained from the different plate theories. As one would expect, the CPT exhibits the largest errors. The longitudinal stress $\bar{\sigma}_{11}(H/2)$ and the transverse normal stress $\bar{\sigma}_{33}(0)$ attain their minima and maxima, respectively, at $p \simeq 2$.

We have listed in Table 3 values of the flexural eigenvalue and the first nine thickness mode eigenvalues for a square Al/ZrO_2 functionally graded thick plate. The results are obtained by using the Mori–Tanaka scheme with the metal as the matrix phase and the ceramic as the particulate phase. The tabulated results should facilitate comparisons between the exact values and those obtained from plate theories or other approximate methods such as the finite element method.

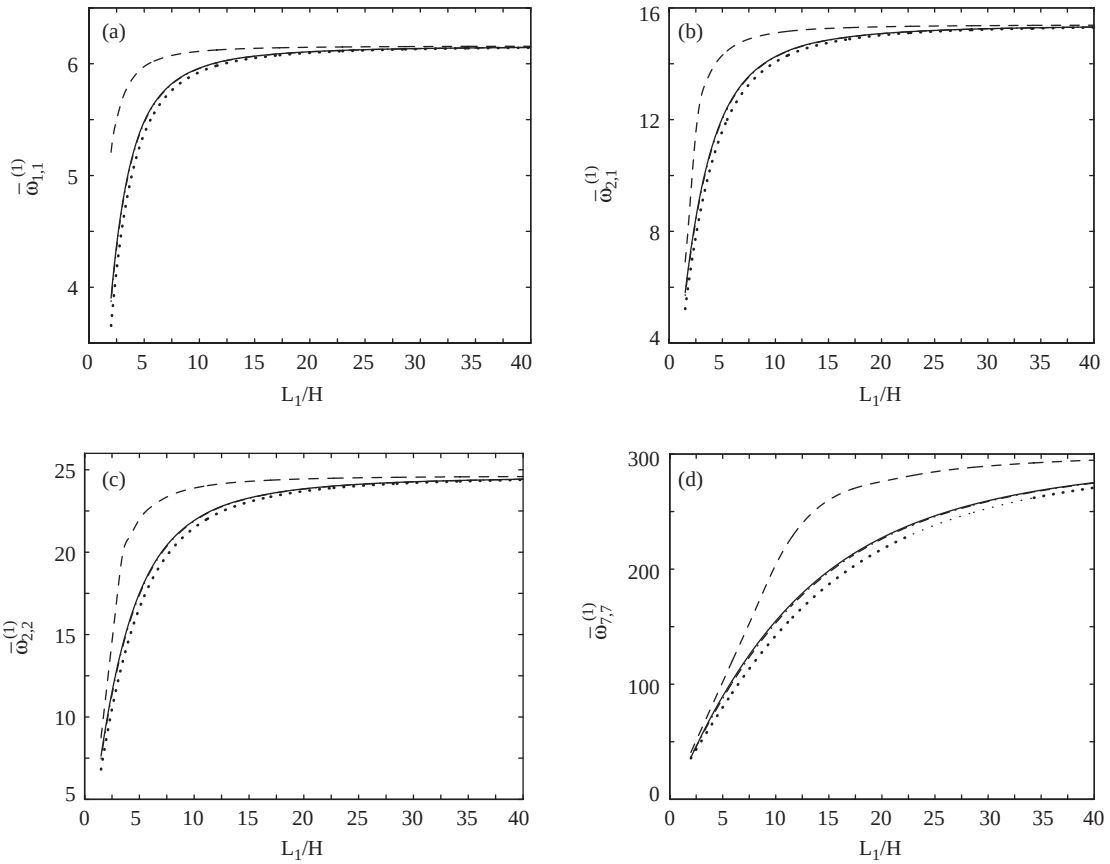

Fig. 5. Flexural mode natural frequency versus length-to-thickness ratio for the Al/ZrO_2 functionally graded square plate computed using the MT_m homogenization scheme and $V_c^- = 0$, $V_c^+ = 1$, $p = 1$: ——, exact; – – –, CPT; – · – · –, FSDT; ·····, TSDT.

According to Batra and Aimmanee [48], pure distortional modes of vibration can occur in a functionally graded plate only when μ/ρ is independent of x_3. Since this is not the case in general, these modes have not been investigated here.

6.3. Functionally graded plate with combined microstructure

In the example problems studied so far, we used a single homogenization scheme, namely the Mori–Tanaka method, to estimate the effective properties for the entire plate. This approach is appropriate only for functionally graded plates that have the same microstructure everywhere. Reiter and Dvorak [31] performed detailed finite element studies of the response of simulated discrete models containing both skeletal and particulate microstructures. They concluded that homogenized models of combined microstructures which employ only a single averaging method do not provide reliable agreements with the discrete model predictions. However, close agreement

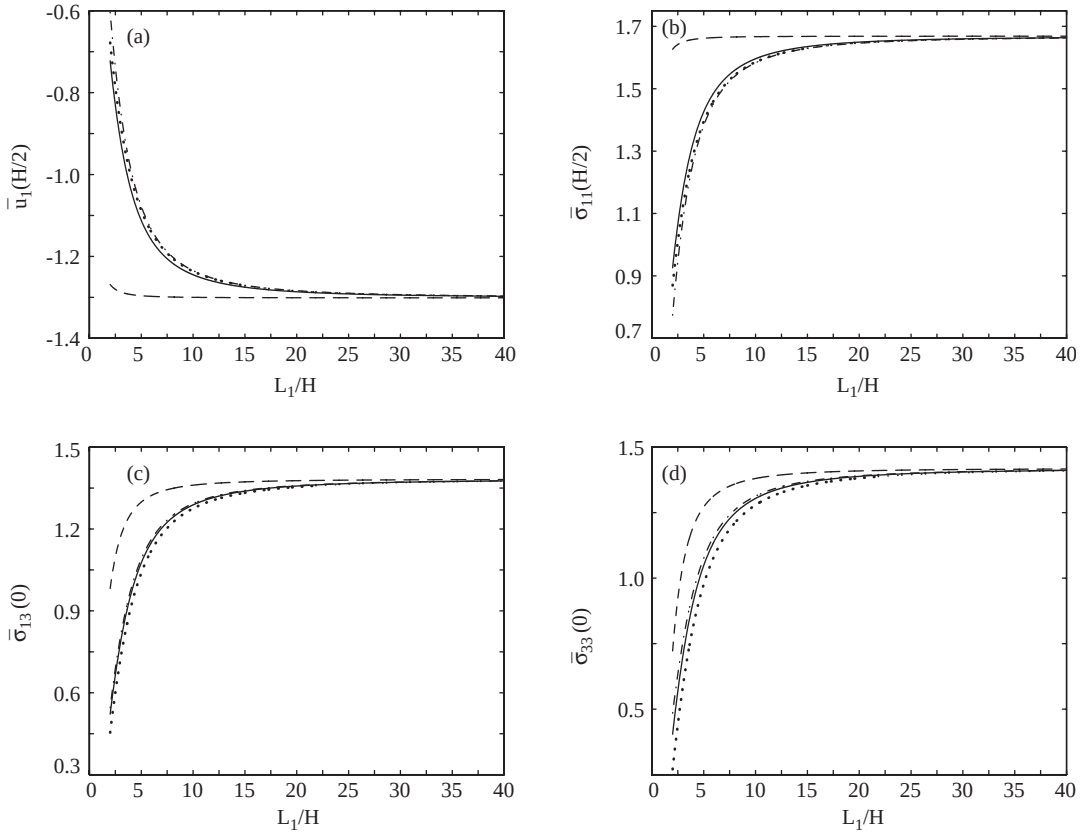

Fig. 6. Non-dimensional (a) axial displacement, (b) longitudinal stress, (c) transverse shear stress and (d) transverse normal stress versus length-to-thickness ratio for the Al/ZrO_2 functionally graded square plate computed using the MT_m homogenization scheme, corresponding to the mode shape $k = 1$, $m = 1$ for $V_c^- = 0$, $V_c^+ = 1$, $p = 1$: ——, exact; – – –, CPT; – · – · –, FSDT; ……, TSDT.

with the discrete model was shown by homogenized models which employ different effective property estimates for regions of the plate that have different microstructures. They state that in those parts of the graded microstructure which have a well-defined continuous matrix and discontinuous reinforcement, the effective properties should be approximated by the appropriate Mori–Tanaka estimates, and in skeletal microstructure that often form transition zones between clearly defined matrix and particulate phases, the effective properties should be approximated by the self-consistent method.

We consider a functionally graded plate that has an affine variation of the ceramic volume fraction given by $V_c = 1/2 + x_3/H$. It is assumed to have a well-defined continuous metallic matrix with discontinuous ceramic particles in the metal-rich region $-0.5H \leqslant x_3 \leqslant -0.2H$ adjacent to the bottom surface and a well-defined continuous ceramic matrix with discontinuous metallic particles in the ceramic-rich region $0.2H \leqslant x_3 \leqslant 0.5H$ adjacent to the top surface. The plate is assumed to have a skeletal microstructure in the central region $-0.2H \leqslant x_3 \leqslant 0.2H$. We use a *combined model*, wherein the effective properties in the metal-rich region adjacent to the bottom

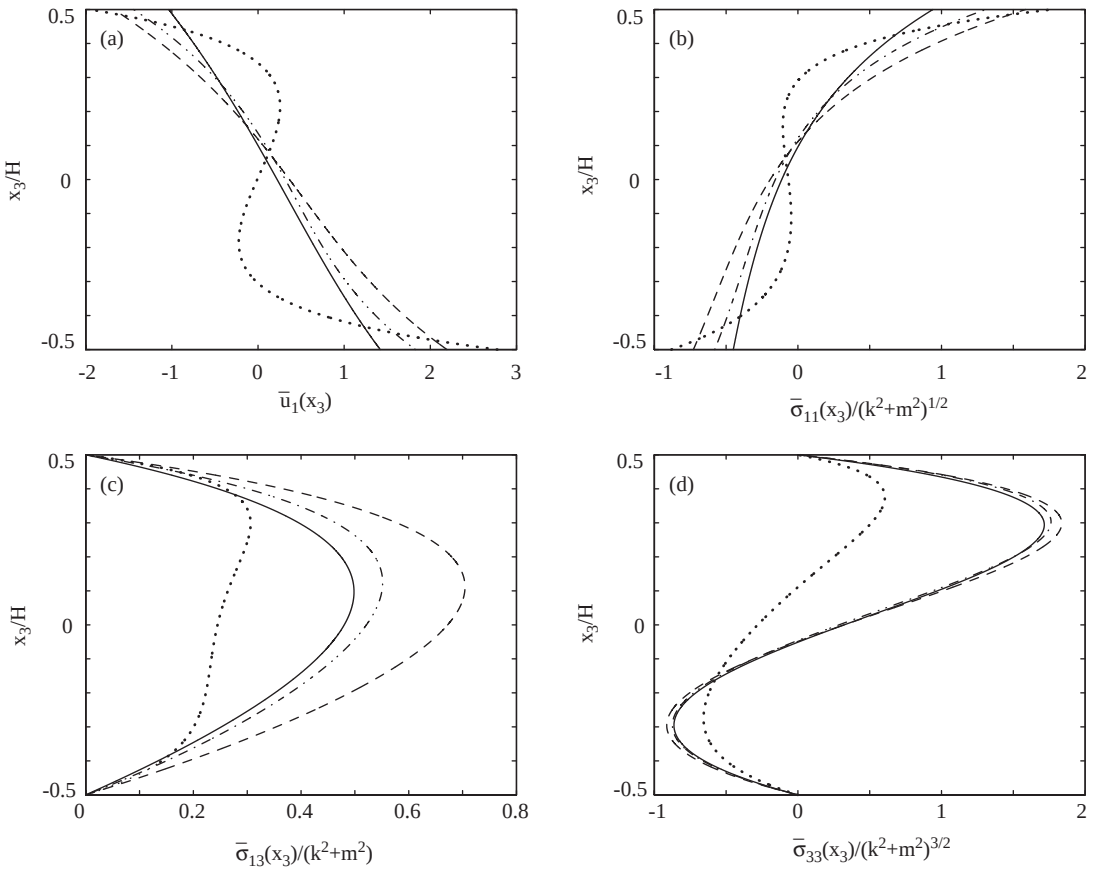

Fig. 7. Through-the-thickness variation of the transverse deflection and stresses in the Al/ZrO_2 functionally graded square plate corresponding to the flexural eigenvalue $\omega^{(1)}_{k,m}$; computed using the MT_m homogenization scheme, $L_1/H = 4$, $V_c^- = 0$, $V_c^+ = 1$, $p = 1$: ——, $k = 1$, $m = 1$; – – –, $k = 2$, $m = 1$; – · – · –, $k = 2$, $m = 2$; ……, $k = 7$, $m = 7$.

surface are obtained by the Mori–Tanaka scheme with a metallic matrix phase (MT_m), the effective properties in the ceramic-rich region adjacent to the top surface are obtained by the Mori–Tanaka scheme with a ceramic matrix phase (MT_c) and the effective material properties in the central region are obtained by the self-consistent scheme (SC). To accommodate discontinuities in homogenized material properties predicted at the boundaries between the different regions, we employ the third order transition functions used by Reiter and Dvorak [31] in transition regions of width $0.05H$ centered at $x_3 = -0.2H$ and $x_3 = 0.2H$. Through-the-thickness variations of Young's modulus and the shear modulus using the combined model for an Al/SiC functionally graded plate are given in Ref. [24].

In the combined model there are five distinct regions in the thickness direction, namely the three primary regions in which the effective properties are obtained by MT_m, MT_c and SC and the two transition regions at the boundaries between them. Within each region the effective material properties are expanded as Taylor series and the solution to the equations of motion are obtained

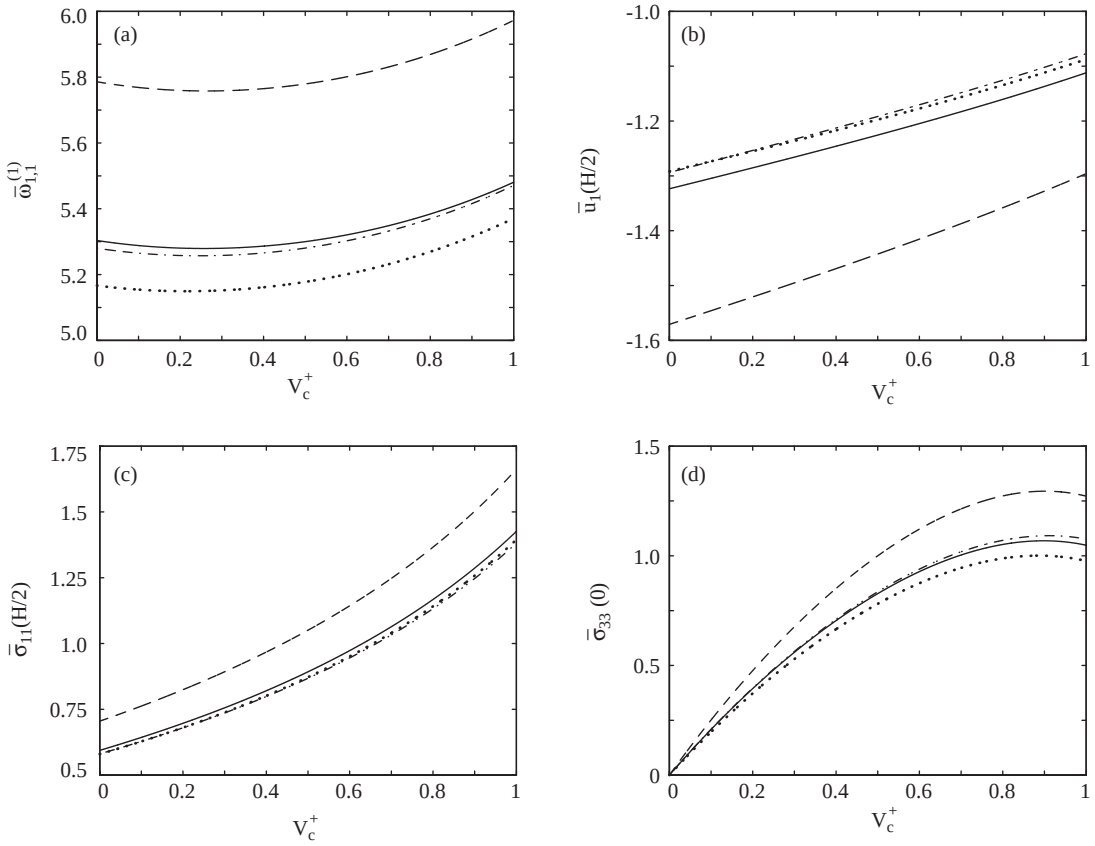

Fig. 8. Flexural frequency, displacement and stresses versus ceramic volume fraction on the top surface, corresponding to the flexural eigenvalue $\omega^{(1)}_{1,1}$ for Al/ZrO_2 functionally graded square plate using the MT_m homogenization scheme, $L_1/H = 5$, $V_c^- = 0$, $p = 1$: ——, exact; – – –, CPT; – · – · –, FSDT; ⋯⋯, TSDT.

in terms of six unknown constants, resulting in a total of 30 unknowns. The constants are determined by satisfying boundary conditions (5) on the top and the bottom surfaces of the plate and interface continuity conditions (6) between adjoining layers. This results in three conditions each for the top and the bottom surfaces and six conditions at each of the four interfaces between regions with distinct micromechanical models. The satisfaction of these conditions gives a system of 30 linear homogeneous algebraic equations for the 30 unknowns. The requirement for this set of equations to have a non-trivial solution gives the equation from which frequencies can be computed.

6.3.1. Free vibrations

A comparison of the flexural frequency $\bar{\omega}^{(1)}_{1,1}$ and the corresponding axial displacement $\bar{u}_1$ and stresses $\bar{\sigma}_{11}$ and $\bar{\sigma}_{33}$ versus the length-to-thickness ratio computed using the combined model and the three single averaging methods is shown in Fig. 10. Results obtained by the combined model and the self-consistent scheme are in excellent agreement. For $L_1/H = 20$, the differences in

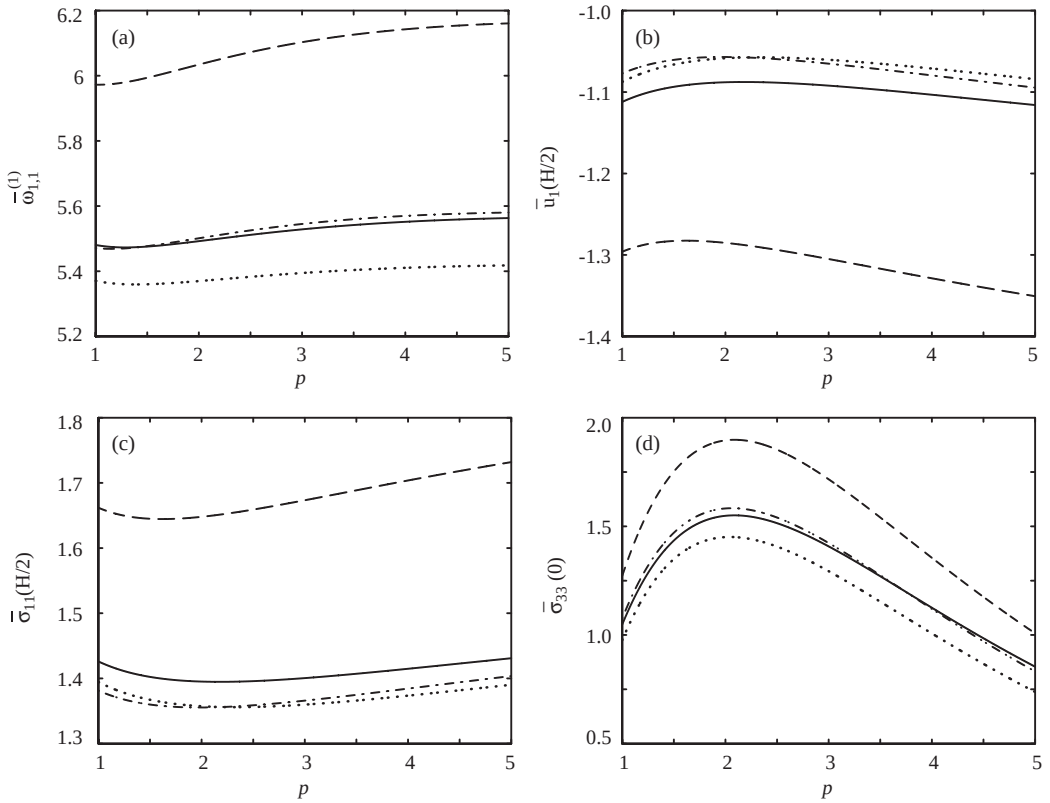

Fig. 9. Flexural frequency, displacement and stresses versus the power-law index p, corresponding to the flexural eigenvalue $\omega_{1,1}^{(1)}$ for Al/ZrO_2 functionally graded square plate using the MT_m homogenization scheme, $L_1/H = 5$, $V_c^- = 0$, $V_c^+ = 1$: ——, exact; – – –, CPT; – · – · –, FSDT; ·····, TSDT.

Table 3
Exact thickness mode natural frequencies a square Al/ZrO_2 functionally graded thick plate

	$V_c^- = 0,\ V_c^+ = 1,\ p = 1$			$V_c^- = 0,\ p = 1,\ L_1/H = 5$			$V_c^- = 0,\ V_c^+ = 1,\ L_1/H = 5$		
Variable	$L_1/H = 5$	$L_1/H = 10$	$L_1/H = 20$	$V_c^+ = 0.3$	$V_c^+ = 0.5$	$V_c^+ = 0.7$	$p = 2$	$p = 3$	$p = 5$
$\bar{\omega}_{1,1}^{(1)}$	5.4806	5.9609	6.1076	5.2799	5.3000	5.3486	5.4923	5.5285	5.5632
$\bar{\omega}_{1,1}^{(2)}$	14.558	29.123	58.250	13.762	13.867	14.065	14.278	14.150	14.026
$\bar{\omega}_{1,1}^{(3)}$	24.381	49.013	98.145	23.071	23.229	23.550	23.909	23.696	23.494
$\bar{\omega}_{1,1}^{(4)}$	53.366	207.50	823.92	50.658	51.115	51.839	50.376	48.825	47.687
$\bar{\omega}_{1,1}^{(5)}$	57.620	212.22	828.78	54.747	55.222	55.986	54.685	53.179	52.068
$\bar{\omega}_{1,1}^{(6)}$	90.993	373.98	1515.0	86.605	87.247	88.399	86.190	83.700	81.825
$\bar{\omega}_{1,1}^{(7)}$	102.97	408.86	1632.4	98.319	99.031	100.25	99.921	98.730	97.384
$\bar{\omega}_{1,1}^{(8)}$	109.37	417.95	1643.3	104.54	105.25	106.51	105.66	104.17	102.71
$\bar{\omega}_{1,1}^{(9)}$	152.63	610.73	2443.3	145.86	146.86	148.62	148.97	147.53	146.02
$\bar{\omega}_{1,1}^{(10)}$	153.39	611.54	2444.1	146.63	147.64	149.40	149.75	148.32	146.85

Effective material properties are estimated by the MT_m scheme.

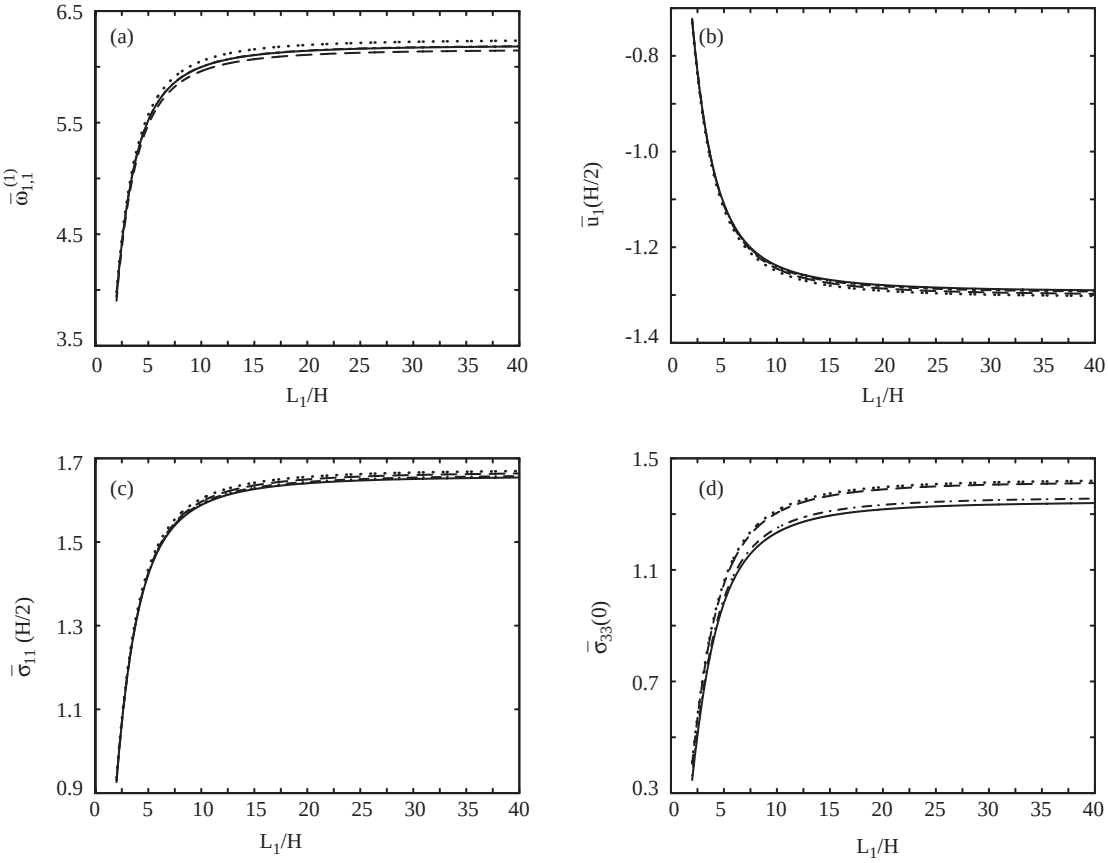

Fig. 10. Non-dimensional (a) flexural frequency $\bar{\omega}^{(1)}_{1,1}$ and corresponding (b) axial displacement, (c) longitudinal stress and (d) transverse normal stress versus length-to-thickness ratio for the Al/ZrO_2 functionally graded square plate computed using various homogenization schemes, corresponding to the mode shape $k = 1,\ m = 1$ for $V_c^- = 0,\ V_c^+ = 1,\ p = 1$: ——, combined; – – –, MT_m; – · – · –, SC; ⋯⋯, MT_c.

$\bar{\sigma}_{11}(H/2)$ between the combined model and that of MT_m, SC and MT_c are 0.56%, 0.21% and 0.93% respectively. The corresponding errors for $\bar{\sigma}_{33}(0)$ are 5.42%, 1.22% and 6.05% respectively. The through-the-thickness variations of the longitudinal stress $\bar{\sigma}_{11}(x_3)$ and the transverse shear stress $\bar{\sigma}_{13}(x_3)$ corresponding to the flexural eigenvalue $\omega^{(1)}_{1,1}$ are shown in Figs. 11(a) and (b). The MT_c homogenization scheme predicts a larger shear stress in the plate than that predicted by the MT_m, the SC and the combined homogenization schemes. The longitudinal and the transverse shear stresses corresponding to the thickness-mode eigenvalue $\omega^{(9)}_{1,1}$ are depicted in Fig. 11(c) and (d). The results obtained from the four homogenization schemes are in good agreement even for the higher thickness modes. Numerical values for the flexural natural frequency $\bar{\omega}^{(1)}_{k,m}$ and associated displacements and stresses obtained by using various homogenization schemes are listed in Table 4. For $L_1/H = 4,\ k = 5,\ m = 3$, the transverse normal stress $\bar{\sigma}_{33}(0)$ is tensile for MT_m and MT_c homogenization schemes, whereas it is compressive for the combined and SC homogenizations. The transverse normal stress $\bar{\sigma}_{33}(0)$ is zero for a homogeneous plate since

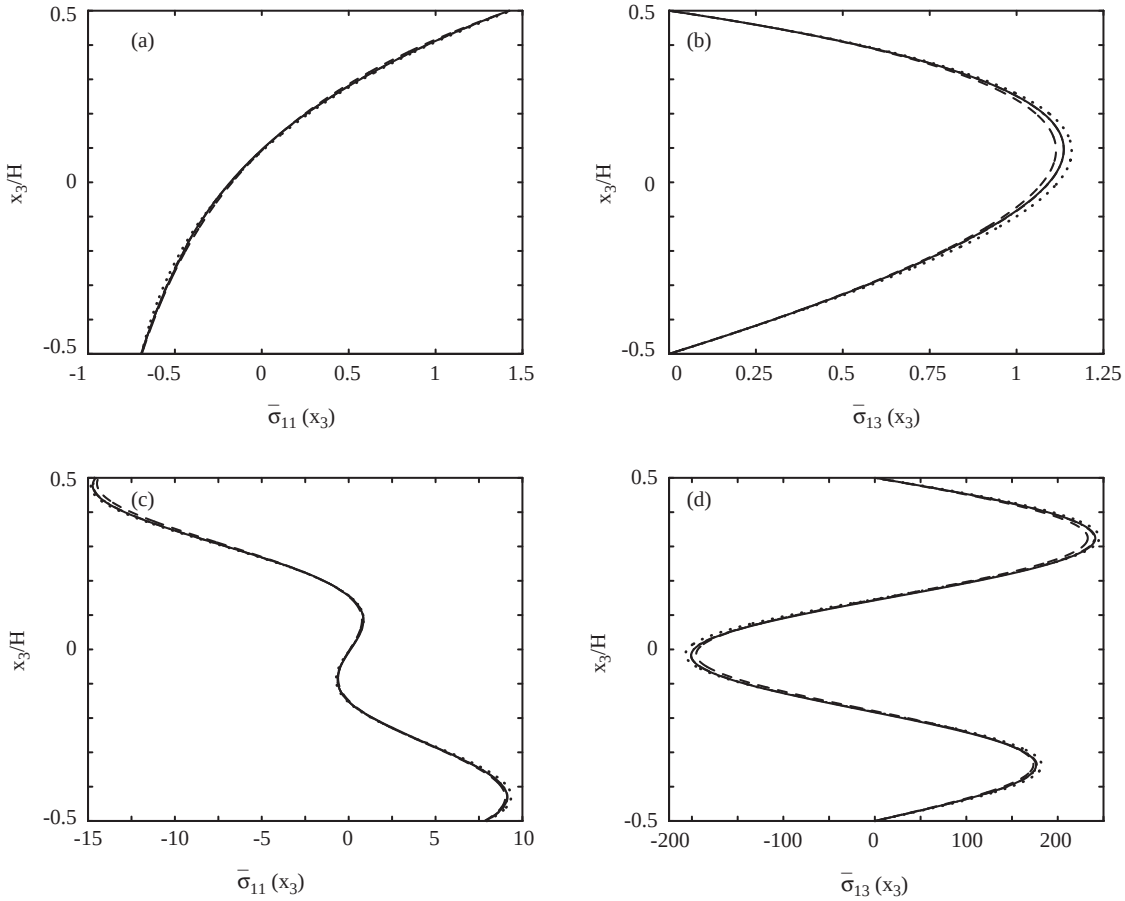

Fig. 11. Through-the-thickness variation of the longitudinal and the transverse shear stresses corresponding to (a,b) flexural mode $\omega_{1,1}^{(1)}$ and (c,d) thickness mode $\omega_{1,1}^{(9)}$ for the Al/ZrO_2 functionally graded square plate computed using various homogenization schemes, $L_1/H = 5, V_c^- = 0,\ V_c^+ = 1,\ p = 1$: ——, combined; – – –, MT_m; – · – · –, SC; ·····, MT_c.

$\bar{\sigma}_{33}(x_3)$ is antisymmetric about the mid-plane. For a functionally graded plate it not antisymmetric and $\bar{\sigma}_{33}(0)$ could be either tensile or compressive depending on the homogenization method used. However, the transverse normal stress at $x_3 = H/4$ is positive for all four homogenization techniques.

6.3.2. *Forced vibrations*

Results for the forced vibration of a thick ($L_1/H = 5$) Al/ZrO_2 functionally graded plate are plotted in Fig. 12 for a static load ($\omega = 0$) and for forcing frequencies $\bar{\omega} = 0.8\bar{\omega}_{1,1}^{(1)},\ 0.95\bar{\omega}_{1,1}^{(1)}$ and $1.05\bar{\omega}_{1,1}^{(1)}$, where $\bar{\omega}_{1,1}^{(1)} = 5.5202$. The combined homogenization scheme is used and the bottom surface is traction free ($q^- = 0$). As expected, the displacements and stresses become larger as the forcing frequency approaches the natural frequency of the plate. Furthermore, the transverse normal stress σ_{33} in the plate can exceed the normal pressure applied on the top surface.

Table 4
Comparison of exact flexural mode natural frequency $\bar{\omega}_{k,m}^{(1)}$ and corresponding non-dimensional displacements and stresses for a square Al/ZrO_2 functionally graded thick plate; $p = 1$, $V_2^- = 0$, $V_2^+ = 1$

Homogenization	$\bar{\omega}_{k,m}^{(1)}$	$\bar{u}_1(H/2)$	$\bar{\sigma}_{11}(H/2)$	$\bar{\sigma}_{11}(-H/2)$	$\bar{\sigma}_{12}(0)$	$\bar{\sigma}_{13}(0)$	$\bar{\sigma}_{33}(0)$	$\bar{\sigma}_{33}(H/4)$
$L_1/H = 4,\ k = 1,\ m = 1$								
Combined	5.2389	−1.0355	1.3278	−0.64032	−0.71496	0.97785	0.84575	4.7902
MT_m	5.1984	−1.0369	1.3296	−0.63645	−0.71594	0.96036	0.91156	4.7100
SC	5.2405	−1.0369	1.3296	−0.63960	−0.71596	0.97862	0.86198	4.7950
MT_c	5.2888	−1.0451	1.3402	−0.63841	−0.72163	1.0014	0.92014	4.9402
$L_1/H = 4,\ k = 2,\ m = 2$								
Combined	15.772	−1.4507	3.7204	−1.6513	−2.0033	4.2682	5.5463	38.830
MT_m	15.611	−1.4443	3.7040	−1.6395	−1.9945	4.1713	6.4729	38.151
SC	15.773	−1.4509	3.7210	−1.6508	−2.0036	4.2705	5.7954	38.929
MT_c	15.937	−1.4614	3.7478	−1.6554	−2.0181	4.3848	6.5761	40.481
$L_1/H = 4,\ k = 5,\ m = 3$								
Combined	40.730	−2.1593	11.799	−4.4641	−4.4727	15.882	−6.3411	205.06
MT_m	40.206	−2.1508	11.753	−4.4108	−4.4550	15.426	7.6242	204.84
SC	40.717	−2.1599	11.803	−4.4611	−4.4740	15.884	−2.2310	207.64
MT_c	41.158	−2.1785	11.905	−4.4777	−4.5126	16.372	9.1099	223.82
$L_1/H = 10,\ k = 1,\ m = 1$								
Combined	5.9980	−1.2387	1.5883	−0.78915	−0.85525	1.3076	1.2338	6.6295
MT_m	5.9609	−1.2448	1.5962	−0.78553	−0.85947	1.2884	1.3042	6.5332
SC	6.0004	−1.2411	1.5914	−0.78804	−0.85693	1.3088	1.2499	6.6341
MT_c	6.0502	−1.2503	1.6033	−0.78456	−0.86329	1.3362	1.3128	6.8078

7. Conclusions

An analytical solution is presented for the vibration of a simply supported functionally graded plate. The effective material properties at a point in the plate are inferred from the volume fractions and material properties of the constituent phases using the Mori–Tanaka method or the self-consistent scheme or a combination of the two. The constituent volume fractions and hence the effective material properties are assumed to vary in the thickness direction only. Suitable displacement functions that identically satisfy boundary conditions at simply supported edges are chosen to reduce the partial differential equations to a set of coupled ordinary differential equations. The effective material properties and the displacements are expanded as Taylor series in the thickness co-ordinate. The ordinary differential equations are solved using the power series method.

The exact solutions for an aluminum/zirconia functionally graded plate are compared with those obtained by the classical plate theory, a first order shear deformation theory and a third order shear deformation theory. For functionally graded thick plates, there are significant differences between the exact solution and results obtained from the classical plate theory even when the transverse shear and the transverse normal stresses are computed by integrating the 3-D elasticity equations. It is found that results from the first order and the third order shear deformation theories compare well with the exact solution. The first order shear deformation

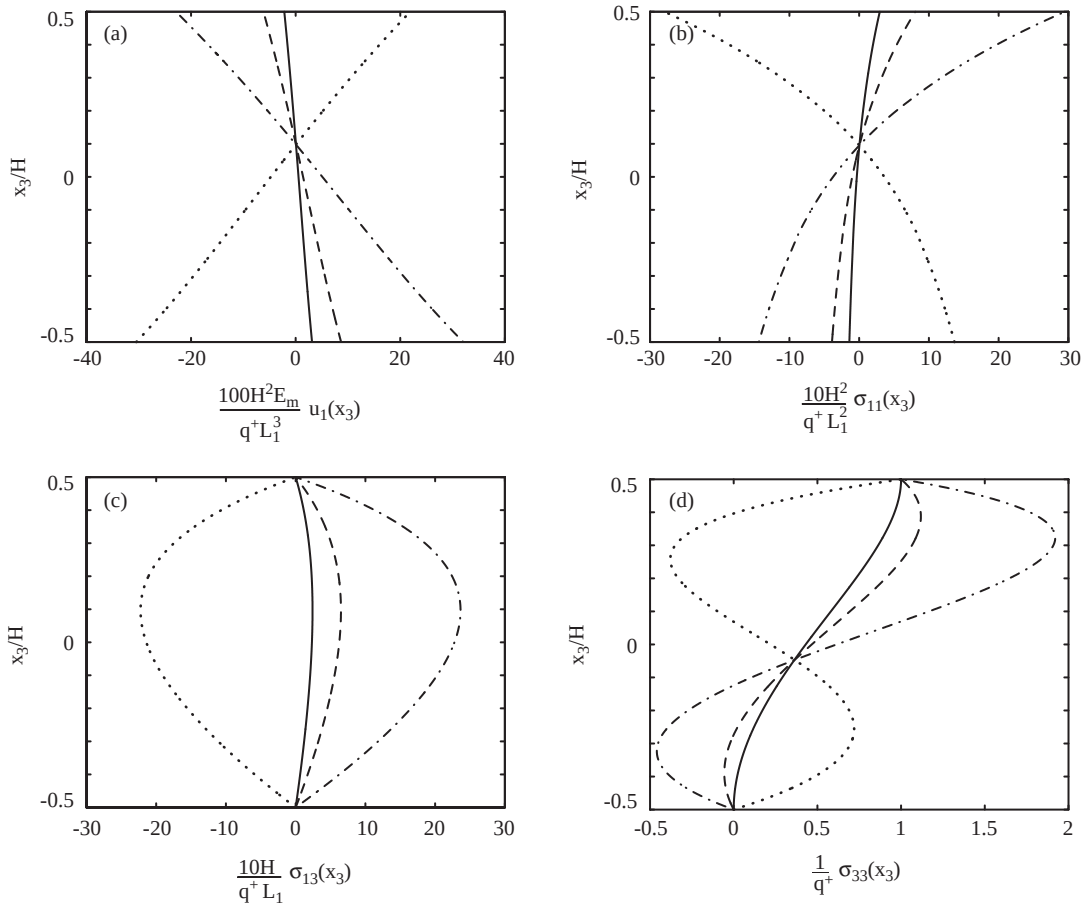

Fig. 12. Through-the-thickness variation of the axial displacement, the longitudinal, the transverse shear and the transverse normal stresses for the forced vibration of the Al/ZrO_2 functionally graded square plate using the combined homogenization scheme, $L_1/H = 5$, $V_c^- = 0$, $V_c^+ = 1, p = 1$, $\bar{\omega}_{1,1}^{(1)} = 5.5202$: ——, $\bar{\omega} = 0$; – – –, $\bar{\omega} = 0.8\bar{\omega}_{1,1}^{(1)}$; – · – · –, $\bar{\omega} = 0.95\bar{\omega}_{1,1}^{(1)}$; ·····, $\bar{\omega} = 1.05\bar{\omega}_{1,1}^{(1)}$.

theory performs better than the third order shear deformation theory for the functionally graded plates studied herein.

The exact solutions presented here provide benchmark results which can be used to assess the adequacy of different plate theories and other approximate methods such as the finite element method. These results have been used by Qian et al. [26,52] to validate their numerical solution obtained with a higher order shear and normal deformable plate theory of Batra and Vidoli [27].

Acknowledgements

RCB's work was partially supported by the ONR Grant N00014-98-0300 to Virginia Polytechnic Institute and State University with Dr. Y.D.S. Rajapakse as the cognizant program manager.

References

[1] R. Berger, P. Kwon, C.K.H. Dharan, High speed centrifugal casting of metal matrix composites, *The Fifth International Symposium on Transport Phenomena and Dynamics of Rotating Machinery*, Maui, Hawaii, May 8–11, 1994.

[2] Y. Fukui, Fundamental investigation of functionally gradient materials manufacturing system using centrifugal force, *JSME International Journal Series III* 34 (1991) 144–148.

[3] K.-L. Choy, E. Felix, Functionally graded diamond-like carbon coatings on metallic substrates, *Materials Science and Engineering A* 278 (2000) 162–169.

[4] K.A. Khor, Y.W. Gu, Effects of residual stress on the performance of plasma sprayed functionally graded ZrO2/NiCoCrAlY coatings, *Materials Science and Engineering A* 277 (2000) 64–76.

[5] A. Lambros, A. Narayanaswamy, M.H. Santare, G. Anlas, Manufacturing and testing of a functionally graded material, *Journal of Engineering Materials and Technology* 121 (1999) 488–493.

[6] E. Breval, K. Aghajanian, S.J. Luszcz, Microstructure and composition of alumina/aluminum composites made by the directed oxidation of aluminum, *Journal of American Ceramic Society* 73 (1990) 2610–2614.

[7] E. Manor, H. Ni, C.G. Levi, R. Mehrabian, Microstructure evaluation of $SiC/Al_2O_3/Al$ alloy composite produced by melt oxidation, *Journal of American Ceramic Society* 26 (1993) 1777–1787.

[8] J.N. Reddy, Analysis of functionally graded plates, *International Journal for Numerical Methods in Engineering* 47 (2000) 663–684.

[9] Z.Q. Cheng, R.C. Batra, Deflection relationships between the homogeneous Kirchhoff plate theory and different functionally graded plate theories, *Archive of Mechanics* 52 (2000) 143–158.

[10] Z.Q. Cheng, R.C. Batra, Exact correspondence between eigenvalues of membranes and functionally graded simply supported polygonal plates, *Journal of Sound and Vibration* 229 (2000) 879–895.

[11] C.T. Loy, K.Y. Lam, J.N. Reddy, Vibration of functionally graded cylindrical shells, *International Journal of Mechanical Sciences* 41 (1999) 309–324.

[12] R.C. Batra, Finite plane strain deformations of rubberlike materials, *International Journal for Numerical Methods in Engineering* 15 (1980) 145–160.

[13] S. Srinivas, A.K. Rao, C.V.J. Rao, Flexure of simply supported thick homogeneous and laminated rectangular plates, *Zeitschrift fur angewandte Mathematik und Mechanik* 49 (1969) 449–458.

[14] S. Srinivas, C.V. Joga Rao, A.K. Rao, An exact analysis for vibration of simply-supported homogeneous and laminated thick rectangular plates, *Journal of Sound and Vibration* 12 (1970) 187–199.

[15] S. Srinivas, A.K. Rao, Bending, vibration and buckling of simply supported thick orthotropic rectangular plates and laminates, *International Journal of Solids and Structures* 6 (1970) 1463–1481.

[16] T.G. Rogers, P. Watson, A.J.M. Spencer, Exact three-dimensional elasticity solutions for bending of moderately thick inhomogeneous and laminated strips under normal pressure, *International Journal of Solids and Structures* 32 (1995) 1659–1673.

[17] J.Q. Tarn, Y.M. Wang, Asymptotic thermoelastic analysis of anisotropic inhomogeneous and laminated plates, *Journal of Thermal Stresses* 18 (1995) 35–58.

[18] Z.Q. Cheng, R.C. Batra, Three-dimensional thermoelastic deformations of a functionally graded elliptic plate, *Composites: Part B* 31 (2000) 97–106.

[19] J.N. Reddy, Z.Q. Cheng, Three-dimensional thermomechanical deformations of functionally graded rectangular plates, *European Journal of Mechanics A/Solids* 20 (2001) 841–855.

[20] J.N. Reddy, Z.Q. Cheng, Three-dimensional solutions of smart functionally graded plates, *Journal of Applied Mechanics* 68 (2001) 234–241.

[21] S.S. Vel, R.C. Batra, The generalized plane strain deformations of thick anisotropic composite laminated plates, *International Journal of Solids and Structures* 37 (2000) 715–733.

[22] P.C.Y. Lee, J.D. Yu, Governing equations for a piezoelectric plate with graded properties across the thickness, *IEEE Transactions on Ultrasonics, Ferroelectrics, and Frequency Control* 45 (1998) 236–250.

[23] P.C.Y. Lee, J.D. Yu, W.H. Shih, Piezoelectric ceramic disks with thickness graded material properties, *IEEE Transactions on Ultrasonics, Ferroelectrics, and Frequency Control* 46 (1999) 205–215.

[24] S.S. Vel, R.C. Batra, Exact solution for thermoelastic deformations of functionally graded thick rectangular plates, *American Institute of Aeronautics and Astronautics Journal* 40 (7) (2002) 1421–1433.

[25] S.S. Vel, R.C. Batra, Three-dimensional analysis of transient thermal stresses in functionally graded plates, *International Journal of Solids and Structures* 40 (2003) 7181–7196.

[26] L.F. Qian, R.C. Batra, L.M. Chen, Static and dynamic deformations of thick functionally graded elastic plates by using higher-order shear and normal deformable plate theory and meshless local Petrov–Galerkin method, submitted for publication.

[27] R.C. Batra, S. Vidoli, Higher-order piezoelectric plate theory derived from a three-dimensional variational principle, *American Institute of Aeronautics and Astronautics Journal* 40 (2002) 91–104.

[28] S.N. Atluri, T. Zhu, A new meshless local Petrov–Galerkin (MLPG) approach in computational mechanics, *Computational Mechanics* 22 (1998) 117–127.

[29] T. Reiter, G.J. Dvorak, V. Tvergaard, Micromechanical models for graded composite materials, *Journal of the Mechanics and Physics of Solids* 45 (1997) 1281–1302.

[30] T. Reiter, G.J. Dvorak, Micromechanical modelling of functionally graded materials, in: Y.A. Bahei-El-Din (Ed.), *IUTAM Symposium on Transformation Problems in Composite and Active Materials*, Kluwer Academic, London, 1997, pp. 173–184.

[31] T. Reiter, G.J. Dvorak, Micromechanical models for graded composite materials: II. Thermomechanical loading, *Journal of the Mechanics and Physics of Solids* 46 (1998) 1655–1673.

[32] T. Mori, K. Tanaka, Average stress in matrix and average elastic energy of materials with misfitting inclusions, *Acta Metallurgica* 21 (1973) 571–574.

[33] Y. Benveniste, A new approach to the application of Mori–Tanaka's theory of composite materials, *Mechanics of Materials* 6 (1987) 147–157.

[34] R. Hill, A self-consistent mechanics of composite materials, *Journal of the Mechanics and Physics of Solids* 13 (1965) 213–222.

[35] Z.H. Jin, R.C. Batra, Some basic fracture mechanics concepts in functionally graded materials, *Journal of the Mechanics and Physics of Solids* 13 (1996) 213–222.

[36] Z.H. Jin, R.C. Batra, Stress intensity relaxation at the tip of an edge crack in a functionally graded material subjected to a thermal shock, *Journal of Thermal Stresses* 19 (1996) 317–339.

[37] Z.H. Jin, R.C. Batra, R-curve and strength behavior of a functionally gradient material, *Material Science & Engineering A* 242 (1998) 70–76.

[38] H. Fröhlich, R. Sack, Theory of the rheological properties of dispersions, *Proceedings of the Royal Society of London A* 185 (1946) 415–430.

[39] R.M. Christensen, K.H. Lo, Solutions for effective shear properties in three phase sphere and cylindrical models, *Journal of the Mechanics and Physics of Solids* 27 (1979) 315–330.

[40] G. Kirchhoff, Über das Gleichgewicht und die Bewegung einer elastischen Scheibe, *Zeitschrift für Reine und Angewandte Mathematik* 40 (1850) 51–58.

[41] E. Reissner, The effect of transverse shear deformation on the bending of elastic plates, *Journal of Applied Mechanics* 12 (1945) 69–77.

[42] R.C. Mindlin, Influence of rotary inertia and shear on flexural motions of isotropic, elastic plates, *Journal of Applied Mechanics* 18 (1951) 31–38.

[43] S.A. Ambartsumyan, in: J.E. Ashton, T. Cheron (Eds.), *Theory of Anisotropic Plates*, Technomic, Stanford, 1970, pp. 176–180.

[44] K.P. Soldatos, Vectorial approach for the formulation of variationally consistent higher-order plate theories, *Composite Engineering* 3 (1993) 3–17.

[45] K.P. Soldatos, Generalization of variationally consistent plate theories on the basis of a vectorial formulation, *Journal of Sound and Vibration* 183 (1995) 819–839.

[46] M. Touratier, An efficient standard plate theory, *International Journal of Engineering Science* 29 (1991) 901–916.

[47] K.P. Soldatos, On certain refined theories of plate bending, *Journal of Applied Mechanics* 55 (1988) 994–995.

[48] R.C. Batra, S. Aimmanee, Missing frequencies in previous exact solutions of free vibrations of simply supported rectangular plates, *Journal of Sound and Vibration* 265 (2003) 887–896.

[49] K.P. Soldatas, V.P. Hadjigergiou, Three-dimensional solution of the free vibration problem of homogeneous isotropic cylindrical shells and panels, *Journal of Sound and Vibration* 137 (1990) 369–384.
[50] R.C. Batra, S. Vidoli, S. Vestroni, Plane waves and modal analysis in higher-order shear and normal deformable plate theories, *Journal of Sound and Vibration* 257 (2002) 63–88.
[51] L.F. Qian, R.C. Batra, L.M. Chen, Elastostatic deformations of a thick plate by using a higher-order shear and normal deformable plate theory and two meshless local Petrov–Galerkin (MLPG) methods, *Computer Modeling in Engineering and Sciences* 4 (2003) 161–176.
[52] L.F. Qian, R.C. Batra, L.M. Chen, Free and forced vibrations of thick rectangular plates by using a higher-order shear and normal deformable plate theory and meshless local Petrov–Galerkin (MLPG) method, *Computer Modeling in Engineering and Sciences* 4 (2003) 519–534.